HTLV-1 Rex hijacks UPF1 in a CRM1 dependent manner, leading to NMD inhibition and revealing unexpected proviral roles of UPF1.

Prochasson L[1], Mghezzi-Habellah M[1], Roisin A[1], Palma M[2], Robin JP[1], de Bossoreille S[1], Sareoua L[3], Cluet D[1], Mouehli M[1], Decimo D[3], Réty S[1], Desrames A[5], Chaze T[4], Matondo M[4], Dutartre H[3], Thoulouze MI[5§], Lejeune F[2], Jalinot P[1], Mocquet V[1*]

[1] Laboratoire de Biologie et Modélisation de la Cellule, Ecole Normale Supérieure - Lyon, Université Claude Bernard Lyon, U1293, UMR5239, France

[2] Univ. Lille, CNRS, Inserm, UMR9020-U1277 - CANTHER - Cancer Heterogeneity Plasticity and Resistance to Therapies, F-59000 Lille, France

[3] Centre International de Recherche en Infectiologie, Ecole Normale Supérieure - Lyon, Université Claude Bernard Lyon, U1111, UMR5308, France

[4] Institut Pasteur, Université Paris Cité, CNRS UAR2024, Proteomics Platform, Mass Spectrometry for Biology Unit, 28, Rue du Docteur Roux, 75015 Paris, France.

[5] Institut Pasteur, CNRS UMR 3569, Biofilm and Viral Transmission Team, Structural Virology Unit, F-75724 Paris, France.(§ present address: INRAE, UE-1277 Plateforme D'infectiologie Expérimentale (PFIE), Centre de Recherche Val de Loire, F-37380 Nouzilly, France)

*vincent.mocquet@ens-lyon.fr

Abstract

The hijacking of CRM1 export is an important step of the retroviral replication cycle. Here, we investigated the consequences of this hijacking for the host. During HTLV-1 infection, we identified the formation of a complex composed of Rex, CRM1 and the RNA helicase UPF1, leading to the nuclear retention of UPF1. We further showed how this leads to the inhibition of the nonsense mediated mRNA decay (NMD), known to have an antiviral function. Corroborating these results, we described a similar process with Rev, the functional homolog of Rex from HIV-1. Unexpectedly, we also found that, for HTLV-1 , this process is coupled with the specific loading of UPF1 onto vRNA, independently of NMD. In this latter context, UPF1 positively regulates several steps of the viral replication cycle, from the nuclear export of vRNA to the production of mature viral particles.

Introduction

The maintenance of cell homeostasis requires a strict control of the repartition of macromolecules between nucleus and cytoplasm. Pathways monitoring this shuttling rely on the nature of the macromolecules to be exported or imported. Notably, whereas bulk mRNA export occurs via the NXF1/TAP1 pathway after its association with TREX complex, the exportin CRM1 (XPO1) mediates the export of proteins containing a Nuclear Export Signal (NES). These cargoes may be associated or not with a specific subset of RNA such as rRNA, snRNA and some mRNA[1,2]. The NES is characterized by a specific stretch of 4 hydrophobic amino acids with variable interspaced amino acids that influences the NES affinity to CRM1. The formation of the complex between CRM1 and the NES containing protein also requires the GTPase Ran to conformationally stabilize the NES binding groove of CRM1[3–6]. However, the affinity of many NES substrates for CRM1 is rather low, suggesting that the formation of this trimeric transport complex is a rate-limiting step in nuclear export[7–9]. At the nuclear pore, Ran GAP catalyses the conversion of RanGTP to RanGDP, inducing the dissociation of the trimeric complex CRM1/Cargo/Ran and the release of the cargo in the cytoplasm. Ultimately, the free CRM1 re-enter the nucleus for a new round of export[10]. Among the plethora of functionally and structurally unrelated protein and RNP cargoes, the mislocalization of several of them due to CRM1 dysfunction supports a role of CRM1 in disease: that is the case of proteins involved in the control of DNA repair, cell cycle, transcription regulation or apoptosis such as BARD1, p21, p27, p53, FOXO3, APC and Survivin[11,12]. In addition, CRM1 overexpression and mutations were directly correlated with multiple types of cancer, notably

acute myeloid leukemia and multiple myeloma[13–16]. As a consequence, CRM1 was considered as a valuable target for anticancer therapies. CRM1 inhibitors where shown to sensitize cancer cells to apoptosis and several of them are currently under clinic trials[17,18].

An important subset of CRM1 cargoes includes proteins involved in RNA processing. Notably, the DNA/RNA helicase UPF1 and its partner UPF2 have been reported to shuttle between cytoplasm and nucleus via CRM1: interactions were identified by mass spectrometry and treatments with the CRM1 inhibitor leptomycin B, induced their nuclear retention[19–21]. However, the impact of a shuttling perturbation on their cellular functions have never been evaluated. UPF1 works at the crossroad of multiple processes for DNA and RNA maintenance and is directly involved in the nonsense mediated mRNA decay (NMD)[22]. NMD targets and degrades mRNA harbouring premature termination codons (PTC) due to the assembly of a NMD promoting complex around UPF1, between the terminating ribosome and a downstream Exon Junction Complex[23–30]. In addition to PTC containing RNA, NMD was shown to target several viral RNA, exerting an intrinsic antiviral function[31–37]. Particularly, the unspliced viral RNA (vRNA) from the human delta retrovirus HTLV-1 is destabilized in a UPF1 and UPF2 dependent manner[38,39]. To counter this threat and fully express their compact genome, virus evolved different bypass strategies[40]. During HTLV-1 infection, the viral proteins Tax and Rex were shown to trans-inhibit NMD[38,39]. Tax directly binds UPF1 and exerts a dual inhibiting effect, repressing its ATPase activity and ultimately NMD[41]. Recently, Nakano et al suggest that the N-terminal domain of Rex as well as its phosphorylation were critical for Rex/UPF1 interaction, leading to the Rex incorporation in NMD complex[42]. A clear mechanism of inhibition is still to be deciphered.

Interestingly, viruses also express NES containing proteins, such as the retroviral protein Rex from HTLV-1[43]. Its role in the vRNA export to the cytoplasm has been extensively studied: Rex interferes with the host splicing machinery, stabilizes vRNA over spliced isoforms and hijacks the cellular shuttling machinery to export vRNA towards translation or viral encapsidation[44–46]. Notably, its Nuclear Localisation Signal (NLS) favors an importinβ–dependent nuclear translocation[47] where it accumulates in the nucleoli and binds the highly basic arginine rich motif of the vRNA called “Rex responsive element (RxRE)” [48]. It also displays a dual multimerization motif encompassing the NES[49]. It was proposed that Rex interacts with CRM1, multimerizes and then binds the vRNA, leading to the export of this mRNP. The cytoplasmic accumulation of vRNA resulting from the hijack of CRM1 then allows the translation of the structural precursor polyprotein GAG and the packaging of two vRNA copies within the newly synthesized viral particles[50].

Unexpectedly, while the causative role of CRM1 in disease strongly stresses the importance of a correct repartition of cargoes between nucleus and cytoplasm, understanding the impact of CRM1 hijacking by retroviral transporters on the cellular homeostasis is barely evoked in the literature. Thus, in this work, we investigated how the hijacking of CRM1 by HTLV-1 Rex affects the relationship between CRM1 and the cargo UPF1, as well as this latter function in the NMD. We found that Rex dependent hijacking of CRM1 is the initial step of an additional hijacking of UPF1: on one hand, Rex stabilizes the UPF1/CRM1 interaction, provokes the nuclear accumulation of UPF1, and represses its association with bulk RNA. As a consequence, this inhibits NMD and the degradation of vRNA. On the other hand, Rex drives UPF1 repositioning on the vRNA, irrespective of NMD. We found that UPF1 stimulates vRNA export and viral particles maturation, ultimately supporting the

infectiveness of the infected cells. Our work thus demonstrates an unexpected pro-viral role of the helicase UPF1 during HTLV-1 infection.

Results

1. Rex interferes with CRM1-dependent export of UPF1

To address how cell functions are impacted by the hijack of CRM1 by Rex, we decided to focus on the RNA helicase UPF1, which nuclear export relies on CRM1. Having verified that UPF1 export effectively depends on CRM1 (**supplementary Fig1**), we first examined the effect of Rex on the formation of CRM1-UPF1 complexes. 293T cells were transfected with combinations of a plasmid encoding Rex and a plasmid expressing a RxRE containing RNA, to mimic the viral RNA export via Rex and CRM1[51]. First, Rex and CRM1 co-immunoprecipitations (coIP) confirmed that Rex binds specifically to endogenous CRM1 and regardless of the expression of the RxRE motif bearing-RNA (**Fig 1a-b)**. This supports the hypothesis that Rex can hijack CRM1 before its binding to viral RNA. Second, we revealed that endogenous UPF1 is able to coIP CRM1 and Rex. Strikingly, the amounts of CRM1 associated with UPF1 are increased when Rex is expressed, suggesting a stabilization of CRM1-UPF1 complex by Rex (**Fig 1c panel (i)**). Moreover, the co-expression of the RxRE containing RNA and/or RNAse treatments didn't modify either the UPF1-Rex association or the UPF1-CRM1 stabilization (**Fig 1c panel (i) and (ii)**). This indicates that the formation of a UPF1-Rex-CRM1 complex can exist independently of RNA, including the RxRE motif bearing-RNA. To confirm and further characterize the role of Rex in stabilizing UPF1-CRM1 interaction, we carried out UPF1 coIP with cells expressing Rex mutants (**Fig 1d**). Rex with a mutation in the Nuclear Export Signal (NES) no longer interacts with CRM1 and is functionally not able to export RNA containing a RxRE motif compared to Rex WT; Rex with a mutation in the Nuclear Localisation Signal (NLS) still interacts with CRM1 but is also greatly impaired in RNA export (**supplementary Fig2b-c**). In addition, the NLS mutation affects the UPF1/Rex association, as shown in UPF1 coIP experiments (**Fig 1d compare lane 2 and 4**). We found that the CRM1/UPF1 association is significantly reduced in both Rex mutants' conditions compared to Rex WT (**Fig 1d** and quantifications in **supplementary Fig2d**). Finally, UPF1 coIP in cells expressing Rex and treated with CRM1 siRNA revealed that Rex is less associated with endogenous UPF1 when CRM1 levels are reduced (**Fig 1e, compared lane 2 to 3**). Altogether, those data suggest that a tripartite complex UPF1/CRM1/Rex is being formed during CRM1 hijack by the retroviral transporter Rex.

To further characterize this complex, we looked at its intracellular distribution by monitoring Rex and UPF1 with Proximity Ligation Assay (PLA), a 40nm resolution technique that detects protein-protein colocalization. In 293T cells expressing HA-Rex, PLA between Rex and endogenous UPF1 displayed numerous foci in the cytoplasm as well as in the nucleus (**Fig 1f and supplementary Fig2a**). Those observations corroborated that Rex can target endogenous UPF1 and that it occurs in the nucleus. Moreover, we wanted to better evaluate the overall cellular localization of UPF1 regarding the expression of Rex. Confocal microscopy experiments showed that in control condition, endogenous UPF1 is mostly cytoplasmic (**Fig 2a-b, panel (i)**). Strikingly, when Rex is expressed, UPF1 is significantly accumulated in the nucleus compared to control conditions. As shown by colocalizing pixel analysis, Rex, CRM1 and UPF1 signals overlap in the nucleus and at the periphery of the nucleus (**Fig 2a-b panel (ii)**). The quantification of the nucleo/cytoplasmic repartition of

UPF1 signal and the percentage of cells with UPF1 nuclear signal in both populations of cells indicate a nuclear retention of UPF1 upon Rex expression **(Fig 2c)**. Thus, these results demonstrated that *in cellula*, the expression of Rex and the further formation of a tripartite UPF1/Rex/CRM1 complex affect UPF1 cellular distribution by retaining a significant part of the UPF1 pool in the nucleus.

2. CRM1 hijacking by Rex interferes with UPF1 function during NMD

To test whether this modification of UPF1 localization by Rex could impact its activity, we focus on one of its well described functions: the nonsense-mediated mRNA decay (NMD). Since UPF1 activity in NMD is functionally linked to its RNA binding capacity, we first investigated this latter by RNA immunoprecipitation (RIP) assays. HeLa cells were transfected with a plasmid coding a NMD sensitive reporter mRNA (Globin PTC, a globin minigene with a premature termination codon in the second exon[52]) as well as increasing amounts of Rex coding plasmids. UPF1 was further immunoprecipitated and the amounts of bound Globin PTC were quantified by RTqPCR. Rex expression as well as UPF1 immunoprecipitations were checked by western blot (**Fig 3a**). When Rex is expressed, the level of Globin PTC associated to UPF1 is significantly reduced compared to conditions without Rex (**Fig 3a**). In addition, to correlate this effect with the formation of the previously described UPF1/CRM1/Rex complex, we also carried out UPF1 RIP experiments in cells transfected with Rex NES mutant coding plasmid. As expected, Rex NES mutant did not affect UPF1 binding capacity to globin PTC compared to Rex WT (**Fig 3b**). This recovery confirms that CRM1 hijacking by Rex leads to UPF1 decreased association to its RNA substrate.

Since NMD requires UPF1 recruitment to RNA to initiate their degradation, we checked whether the defect of UPF1 binding on RNA upon Rex expression could correlate with NMD inhibition. To do so, we analysed the decay rate of the Globin PTC with or without Rex expression by monitoring the RNA levels after cell exposure to the transcription inhibitor DRB. Here, Rex expression led to a significant decrease in the decay rate of Globin PTC (**Fig 3c, compare red and purple bars**). To control the specificity of this result, the decay rate of a NMD unsensitive RNA (Globin WT, a globin minigene without premature termination codon) was analysed as well. As expected, without Rex, the decay rate of Globin WT is lower than that of Globin PTC (**Fig 3c, compare blue and red bars**). When Rex is expressed, the decay rate of Globin WT is unaffected (**Fig 3c, compare blue and green bars**) and is of similar value as that of Globin PTC (**Fig 3c, compare green and purple bars**). The expression of a RxRE containing RNA did not significantly modify Rex' impact on the Globin PTC decay rate (**Fig 3c, compare purple and orange bars**). Finally, by using the sunset assay (see methods), we confirmed that these observations are not related to a possible translation inhibition by Rex (**Fig 3d**). These results demonstrate that Rex specifically and efficiently inhibits NMD.

To correlate this Rex dependent NMD inhibition with our previous observations, we analysed the effect of the Rex NES mutant on Globin PTC mRNA half-life (as another indication of NMD efficiency). Consistently with previous results, Globin PTC half-life is significantly increased by Rex WT expression compared to control condition (9.9h *vs* 2.9h) reflecting NMD inhibition. Conversely, Rex NES loss its ability to inhibit NMD as showed by the restored Globin PTC half-life (3.8h). As a control, we also monitored the effect of Rex NLS mutant, that couldn't either support NMD inhibition (2.3h). Interestingly, the co-

expression of NES and NLS mutants did not restored NMD inhibition (1.9h), suggesting that the presence of Rex both in nucleus and cytoplasm is not sufficient for NMD inhibition but that its shuttling capacity is required (**Fig 3e**).

Altogether, these results demonstrate that Rex expression and shuttling lead to a diminution of UPF1 association with RNA, which correlates functionally with NMD inhibition.

3. CRM1 hijacking by other retrovirus also interferes with UPF1 cellular localization and its NMD function.

CRM1 hijacking is a hallmark of several complex retroviruses[44]. For instance, HIV express Rev, a functional homolog of HTLV Rex; although these proteins share low sequence homology, they both display similar functional domains such as RNA binding domain, NLS, dual multimerization domain and NES. Rev also shuttles between nucleus and cytoplasm, hijacks CRM1 and exports the unspliced viral RNA[53]. In order to reinforce our observations supporting an impact of CRM1 hijacking on UPF1 activity, we investigated the impact of Rev expression as we did previously with Rex. Interestingly, a UPF1/Rev/CRM1 complex has already been described[54]. Thus, we directly looked at the endogenous UPF1 intracellular distribution under Rev expression by confocal microscopy. Rev strongly colocalizes with UPF1 and CRM1 in nucleolar compartments (**Fig. 4a (i) and supplementary Fig3a**). As for Rex, a significant nuclear retention of UPF1 can be quantified when Rev is expressed compared to control condition (**Fig 4a (ii)**). To further compare Rex and Rev impact on UPF1, we checked whether the Rev-mediated nuclear relocalisation of UPF1 can be also correlated with NMD inhibition. We found an increased half-life of Globin PTC after Rev expression compared to control condition (4.3h *vs* 1.6h, **Fig 4b**) suggesting that Rev is able to inhibit NMD and to alter the stability of non-viral RNAs. Moreover, as Rev-mediated inhibition of NMD is reported here for the first time, we further characterized the specificity of our observations: first, we excluded that they were related to a translation defect by carrying out a sunset assay, as previously done for Rex (**Supplementary Fig3b**). Second, we monitored Rev impact on the decay rate of Globin WT and compared it to Globin PTC. As expected, the decay rate of Globin WT was not much affected by Rev expression while that of Globin PTC was significantly decreased (**Fig 4c**). Furthermore, to determine whether these observations could be verified in the context of HIV-1 infection, we analyzed HeLa cells pre-transfected with Globin reporters and infected for 48h with HIV-GFP lentiviral particles (HIV) or lentiviral particles expressing GFP only (VLPCtr) as control. While the decay rate of Globin WT was not affected by HIV infection, that of Globin PTC was significantly reduced, indicating that HIV infection is able to inhibit NMD **(Fig 4d**). Altogether, these results demonstrate a specific NMD inhibition during HIV infection, which occurs at least in a Rev-dependent manner.

Consistently with our previous results on Rex, UPF1 RIP experiments revealed that Rev expression is also associated with a decrease in UPF1 association with the Globin PTC or the Globin WT mRNAs (**Fig 4e and 4f respectively**). To reinforce these observations, the association of UPF1 with endogenous NMD sensitive (*smg5* and *gadd45a*) and NMD unsensitive (*gapdh*) RNAs was also investigated. We observed the same decrease in UPF1 association with these endogenous RNA (**Fig 4g**). These results indicate that Rev, like Rex, decreases/prevents UPF1 binding to all RNA, including NMD-sensitive RNAs, consistent

with an early inhibition of the NMD process. Although CRM1 export essentially target protein cargos and not bulk RNA, one can hypothesize that these results illustrate a defect in RNA export rather than a defect in UPF1 accessibility. To eliminate this possibility, we carried out fractionation of cells expressing Rex, Rev or an empty vector and quantified the Nuclear/Cytoplasmic ratio of the previously studied RNA: viral proteins expression did not modify the nucleo/cytoplasmic RNA repartition (**supplementary Fig3c**).

Here, we found that HIV Rev, known to hijack the CRM1 export pathway as does HTLV Rex, induces the nuclear re-localisation of UPF1. Like Rex, Rev provokes a decrease in UPF1 recruitment to RNA that is correlated with the inhibition of NMD.

4. CRM1 hijacking by Rex in HTLV-1 transformed cell line leads to UPF1 relocalization

So far, we demonstrated that independently of the presence of unspliced viral RNA (vRNA), Rex can form a tripartite complex with CRM1 and UPF1, strongly stabilizing UPF1/CRM1 interaction. We correlated the formation of this complex with the nuclear retention of UPF1 and the NMD inhibition. In order to investigate this process in physiological relevant cellular models, we used three HTLV-1 chronically infected CD4+ T cell lines: C91PL and HUT102 that express Rex protein, as well as C8166 that displays a defect in Rex expression, as confirmed by western blot and confocal microscopy (**Fig 5a** and **supplementary Fig4b**). As a negative control we also used uninfected Jurkat CD4+ T cells. CoIP experiments confirm that in the Rex expressing cells, UPF1 interacts with Rex as well CRM1 in higher proportions than in the absence of Rex (**Fig 5a, compare lanes 1-2 to 3-4**). Then, we examined the intracellular distribution of UPF1 and CRM1 in C91PL and C8166 by confocal microscopy (**Fig 5b and supplementary Fig4a**). We found a nuclear retention of UPF1 in ~75% of C91PL compared to ~30% in C8166 cells **(Fig 5b panel (ii))**. Noteworthy, overlapping perinuclear foci of UPF1 and CRM1 were also observed in C91PL only (white arrow in Fig 5b).

In the context of HTLV infection, the direct correlation between intracellular cell redistribution of UPF1/CRM1 and NMD inhibition is made difficult because both C8166 and C91PL cells express the viral protein Tax, another NMD inhibitor that we characterized in the past[38,41]. The expression of Tax in these cell lines is well documented [38,55] . In these cell lines, Tax localization is not specifically linked to either Rex or CRM1 distribution profiles (**supplementary Fig4b-c** and [56]). To evaluate NMD efficiency in a close model, we measured the half-life of the Globin PTC reporter in HeLa cells transfected with different mutated versions of a HTLV molecular clone. As expected, we found that molecular clones deficient for Rex alone (mimicking C8166 cells) or for Tax alone inhibited NMD at similar levels than a WT clone (mimicking C91PL cells) (**supplementary Fig4d**), consistent with our previous finding that NMD is effectively inhibited in C91PL cells compared with Jurkat [38]. These results indicate that both Rex and Tax exhibit an NMD inhibition activity of comparable magnitude in an infectious context.

5. UPF1 is addressed to vRNA in a Rex dependent manner

Unlike HeLa and 293T cells, C91PL cells constitutively express viral RNA. Knowing that the Rex/CRM1 complex binds selectively to unspliced viral RNA (vRNA) to drive its nuclear export, and that Rex and CRM1 modify UPF1 localisation and function, we

questioned the interplay between UPF1 and vRNA. First, we carried out UPF1 RIP experiments in C8166 and C91PL cells, as well as in Jurkat T cells as a negative control. Interestingly, we found that UPF1 RIP were specifically enriched in vRNA in the Rex expressing cells only (**Fig5c, supplementary Fig4e**). To confirm that this association is not related to NMD activation, we carried out RIP targeting UPF2, a NMD cofactor of UPF1, as well as UPF1, Rex or CRM1 as controls. We found no enrichment of vRNA after UPF2 RIP in C91PL compared to C8166, in contrast to the RIP targeting UPF1 and Rex (**Fig 5d**). In addition, we performed UPF2 coIP in C91PL extracts: an interaction between UPF2 and CRM1 was found as expected since UPF2 is a known cargo of CRM1. However, no specific association between Rex and UPF2 could be found, unlike UPF1 (**Fig 5e**). Then, we asked whether UPF1 and Rex can bind concomitantly to vRNA. To do so, we carried out double-RIP experiments. First, a RIP targeting a transiently expressed HA-tagged UPF1 was performed (**Fig 5f, blue bar**). Cells without HA-UPF1 expression were used as a control. Second, RNAs were natively eluted and further subjected to a second RIP against Rex (**Fig 5f, green bar**) or using a control immunoglobulin. RTqPCR on each RIP revealed a significant enrichment of vRNA associated to UPF1 as well as Rex, but to a lower amount. Thus, UPF1 can be recruited on vRNA concomitantly with Rex, in a Rex-dependent manner but independently of its NMD function. To clarify if this recruitment is controlled by the formation of the previously characterized CRM1-UPF1-Rex complex , RIP experiments were carried out on 293T cells transfected with the HTLV-R23L molecular clone (deficient for Rex expression) complemented with plasmids encoding Rex WT or NESmut. As a reminder, we have previously shown that Rex NESmut cannot support the formation of the CRM1/UPF1/Rex complex (**Fig 1e**). RIP Rex experiments showed similar enrichment of vRNA with Rex WT and NES mutant proteins. In contrast, enrichment of vRNA in the UPF1 RIP was drastically reduced with the Rex NES mutant compared with the WT Rex protein (**Fig 5g**). Altogether, these results indicate that in an infectious context, hijacking of CRM1 by Rex drives the loading of UPF1 onto vRNA independently of the NMD process.

6. UPF1 supports different steps of HTLV-1 replication cycle leading to the production of viral particles.

In this context, we hypothesized that the relocalization of UPF1 on vRNA induced by Rex and CRM1 might have a proviral function, contrasting with its antiviral function exerted on NMD. First, we investigated vRNA export. To do so, 293T cells were transduced with lentivectors expressing a doxycycline inducible UPF1 shRNA or a control shRNA. Cells were then treated twice with doxycycline to ensure the lowest levels of UPF1, prior to expression of Rex and a Luciferase reporter to monitor Rex-dependent export (FLucRxRE)[51]. As shown in **supplementary Fig2c** and **Fig 6a**, in the presence of UPF1, Rex is required for the correct export of FLucRxRE RNA, resulting in Firefly luciferase expression. Reduced levels of UPF1 (shUPF1) were associated with a decrease in Firefly luciferase expression. Accordingly, these results reveal a positive role for UPF1 in promoting Rex-dependent export of vRNA.

As previously mentioned, the fate of cytoplasmic vRNA is to be translated into structural viral proteins and enzymes or encapsidated in viral particles. Having demonstrated the loading of UPF1 on viral RNA, we wondered whether this might promote the accumulation of UPF1 at viral particle budding sites. First, we monitored the localisation of the viral matrix (MA/p19) and UPF1 in infected T cells. As expected, C8166 cannot express p19 due to a

defect in Rex expression. In C91PL, p19 is displayed as foci at the cell periphery corresponding to the accumulation of virions on the cell surface[57] (**Fig 6b (i)**). The immunostaining profiles of UPF1 and p19 IF overlap at these foci (**Fig 6b (ii)**). This suggests that UPF1 is present at budding sites and could be incorporated into viral particles. To address this point, we isolated the extra cellular fraction (ECF) of $15x10^6$ infected cells, which contains most of the viral particles produced by the cell, forming a viral biofilm bound to the cell membrane as described previously[57,58]. The presence of viral particles was detected in C91PL only, as shown by monitoring p19 using western blot. The exclusion of cellular contamination of ECF was controlled by probing the cytoplasmic protein RRM2 (**fig 6c**). Finally, UPF1 was identified in ECF from C91PL, but not on that of C8166 or controlled non-infected cells (**Fig 6c**). To confirm the presence of UPF1 in all types of viral particles produced by C91PL infected cells, mass spectrometry experiments were performed on C91PL ECF (cell-associated virions contained in viral biofilms) as well as purified virions released in C91PL culture supernatants (named"free particles"). UPF1 was detected in both fractions. As expected, UPF2 and RRM2 cannot be detected (**Fig 6d**). We performed the same experiments with uninfected CEM T cells known to produce membrane bound and released extracellular vesicles (**supplementary Fig 5a)** [59,60].We found that, although UPF1 is present in both fractions derived from uninfected cells, its relative enrichment in the “free particles” fraction of infected cells is much greater than in uninfected ones **(supplementary Fig 5b-c)**. Altogether, these data confirm the presence of UPF1 in viral particles.

Next, we evaluated the effects exerted by UPF1 during viral particles formation steps. To do so, we proceeded with UPF1 extinction before the expression of a replicative HTLV molecular clone in 293T cells. Viral protein and vRNA from whole-cell extract or from the ECF were analysed (**Fig 7a**). First, western blots showed that the levels of the GAG precursor, encoded by vRNA, were similar with or without UPF1(**Fig 7b panel (i)**). During viral particle formation, GAG maturation leads to its proteolytic cleavage into the nucleocapsid (NC/p15), the matrix (MA/p19) and the capsid (CA/p24). Unexpectedly, we observed by western blot that mature p19 and p24 were less present in whole-cell extracts deprived from UPF1 **(Fig 7b panel (i))**. To confirm this, FACS was performed on permeabilized cells using antibodies against UPF1 or p19. UPF1 knock-down was associated with a ~50% decrease in the p19 mean fluorescence (**supplementary Fig6b, c**). We also performed ELISA on whole-cell extracts as well as on the corresponding ECF. In both fractions, UPF1 decrease was associated with weaker p19 signals (**Fig 7c, d**). Western blots and qRT-PCR confirmed that ECF from UPF1-depleted cells contained less p19, p24 and vRNA **(Fig 7b (ii), 7e-f**). However, western blot on the ECF showed that the levels of viral envelope (Env) were less, if at all, affected by UPF1 knock-down **(Fig 7b(ii))**. Corroborating that observation, FACS analysis performed on non-permeabilized cells using the anti-HTLV serum or an anti-Env antibody did not reveal a significant decrease of the cell surface mean fluorescence **(supplementary Fig6b**). Finally, we evaluated the impact of these modifications on HTLV viral particles infectivity and transmission. HTLV-1 transmission occurs via cell to cell contact, through viral biofilm in which viral particles are accumulated, and drastically improve the transmission rate[57]. To assess the impact of UPF1 depletion on HTLV infectivity and spread, co-cultures between C91PL (expressing or not a UPF1 shRNA) and Jurkat-Luc reporter cells (expressing luciferase under the HTLV LTR) were performed as previously described[57]. The significant reduction of UPF1, obtained after 6 days of shRNA induction, was associated with a decrease in p19 levels, consistent with our results on HTLV infected

293T cells (**supplementary Fig 6c**). Under these conditions, the decrease in UPF1 levels resulted in a drastic reduction (~ 60%) of viral transmission to uninfected Jurkat cells after 24 hours of co-culture (**Fig 7g**). Overall, these results showed that UPF1 defects uncouple the levels of structural proteins produced by infected cells, affecting the assembly or maturation of HTLV-1 viral particles and, ultimately, their capacity to transmit infectious virions to neighboring cells.

In conclusion, we demonstrated that UPF1 can be loaded on HTLV vRNA in a Rex dependent manner and exerts functions independent of the NMD process that promote viral replication.

Discussion:

By regulating intracellular distribution of hundreds of proteins and some specific RNA species, CRM1 export pathway is an important process controlling cellular homeostasis. In line with this, CRM1 is a therapeutic target in many human diseases. As introduced earlier, complex retroviruses like HTLV-1 and HIV-1 use retroviral transporters, respectively Rex and Rev, to export their viral RNA via CRM1. While the mechanistic steps of this export are already well described, the cellular consequences of CRM1 hijacking have not been addressed yet. Here, we sought to characterize how hijacking of CRM1 by Rex could affect the NMD, a well described RNA quality control and post-transcriptional process also involved in cellular homeostasis, knowing that its core factor UPF1 is a CRM1 cargo.

We observed that Rex impacts CRM1-dependent UPF1 export through the formation of a UPF1-Rex-CRM1 complex. Our data show that this complex relies on the combined interactions between UPF1 and CRM1, Rex and CRM1 as well as Rex and UPF1, leading to increased levels of CRM1 associated to UPF1. Hypothesizing that we face a sequestration complex, confocal microscopy analysis confirm that while UPF1 is usually mostly cytoplasmic due to an efficient/active nuclear export[21,61], Rex expression indeed promotes UPF1 nuclear accumulation. Consistently with UPF1 improper localization and the current model of NMD, in which UPF1 binds its target in the cytoplasm, we were able to correlate the formation of this sequestration complex with a defect in UPF1 binding to RNA. Finally, we linked these alterations with NMD efficiency: NMD was repressed under Rex expression as shown previously[39] but more interestingly, by using selected Rex mutants, we were able to correlate this inhibition with the formation of the sequestration complex and the capacity of Rex to shuttle with CRM1. Concomitant expression of an RNA containing a RxRE motif gave similar results, meaning that this inhibition process can occur independently of Rex binding to viral RNA and suggesting that RNA binding is not essential to induce Rex shuttling[49]. In addition, similar results were obtained in HTLV-1 chronically infected cells, confirming their physiological relevance.

Recently, *Nakano et al* published that overexpressed UPF1 can interact with Rex in the cytoplasm and P-bodies and that inhibition of NMD depends on several domains of Rex including its Nter part (ARM NLS and X domains)[42]. Our results support and complete theirs: first, we report an interaction between Rex and endogenous UPF1, which is sensitive to a mutation in the NLS domain of Rex. Interestingly, PLA experiments confirm that this interaction occurs in the cytoplasm as well as in the nucleus. While the cytoplasmic presence of these complexes matches with the model of *Nakano et al*, suggesting that Rex may be recruited to NMD complexes via UPF1, the existence of nuclear complexes support an

additional accumulation of UPF1 in the nucleus under Rex control. The modification of UPF1 nuclear export fitness in a Rex dependent manner reduces the ability of UPF1 to bind RNA, further preventing NMD initiation. Thus, we reveal a second model for the Rex mediated NMD inhibition, specifically based on the ability of Rex and UPF1 to be exported by CRM1.

In order to reinforce the demonstration that CRM1 hijacking by a retroviral transporter can alter cellular pathways, we also investigated the effect of HIV Rev: Rev is the functional homolog of Rex encoded by HIV-1 but the two share little sequence identity. Although the sequential steps leading to the formation of an export complex with Rex and Rev may diverge[43,46,57], both result in the formation of a viral transporter multimer interacting with vRNA and CRM1. As expected, Rev expression led overall to similar observations, although some mechanistical discrepancies may account for the slight differences we were able to observe: strikingly, Rev induces a stronger UPF1 nuclear retention, essentially in nucleolus, while UPF1 staining in the presence of Rex was essentially diffuse in the nucleus. Interestingly, this demonstration also points out for the first time that HIV is able to trans-inhibit NMD in a Rev dependent manner, affecting the stability of non-viral RNA. In the cell, NMD exerts an important role during post-transcriptional regulation of gene expression. Notably, it controls pathways involved in the equilibrium between proliferation and differentiation, stress response and immune response. With regards to this role, it is expected that CRM1 hijacking by Rex and Rev will lead to specific post-transcriptional deregulations due to NMD inhibition. Some of these deregulations have already been addressed[62] but a dedicated study is still needed to unravel the significance of these effects during viral infection.

During HIV-1 replication, UPF1 is involved in HIV vRNA export with Rev and CRM1; moreover, in silico protein-protein docking analyses suggest that these interactions occur in a region that overlaps with the UPF2 binding site of UPF1, thereby protecting vRNA from NMD activation[54,63]. UPF1 does not affect the viral particle formation but is encapsidated and favors viral transmission[64]. Considering HTLV, although the UPF1/CRM1/Rex sequestration complex can form without vRNA, we found that it also leads to UPF1 loading on the vRNA exported by Rex in infected cells. This recruitment is not linked with NMD activation, since we observed that it occurs independently from UPF2. The degradation of vRNA by NMD process was shown to involve another pool of UPF1 complexes, containing UPF2[39]. On the contrary, we clearly established that UPF1 plays a positive role in the Rex-dependent vRNA export. Furthermore, we found that in the absence of UPF1, the maturation of structural proteins MA(p19) and CA(p24) was impaired. This reduction is unlikely to be due to the repression of vRNA export since the GAG precursor (pr53GAG) levels were barely affected. However, a decrease in MA and CA levels was observed in cell extracts as well as in the extra cellular fraction where infectious viral particles accumulate. Importantly, the expression of the viral envelope was not significantly affected. Altogether, those observations revealed a role of UPF1 in establishing a correct balance between the different structural proteins that compose the viral particle. We may hypothesize that at the site of viral particles budding, UPF1, bound to vRNA, controls specific maturation steps leading to the production of complete, infectious virions. In support of this hypothesis, we provided evidence that (i) UPF1 is itself loaded into viral particles and that in its absence, vRNA are less incorporated in the viral particles; (ii) viral infectivity from C91PL was clearly repressed when UPF1 levels were reduced. The importance of helicases during the packaging steps has been reported for some viruses in the past: Rep52/40 DNA helicases from AAV-2

are required to translocate single-stranded DNA genomes into preformed empty capsids[65] while NS3 is required for the packaging of YFV vRNA[66]. Retroviruses that lack viral helicases rely on the host's ones : DDX6 is re-directed to the assembly site of foamy virus particles and drags vRNA into them[67]; for HIV, DDX6 directly facilitates capsid assembly while DDX24 promotes the packaging of viral RNA[68]. The new function revealed in this work for UPF1 during HTLV-1 maturation might be in line with this. However, deciphering the underlying molecular mechanisms will require further investigation.

Finally, this work also reveals unexpected data on the regulation of NMD: in the past, the nuclear import of UPF1 by the importin β1 was stressed out as a critical step of the process[69]. Here, the expression of viral proteins shows that modulation of the CRM1 dependent export also impacts on NMD, underscoring the importance of the nucleo/cytoplasmic shuttling process as a node of NMD regulation. Further investigations are needed to understand how the NMD can be controlled at this step in the absence of viral infection.

In conclusion, these results demonstrate that the process of CRM1 subjugation by retroviral transporters can affect cellular pathways. Notably it trans-inhibits the NMD via the formation of a sequestration complex trapping UPF1. Unexpectedly, the hijacked UPF1 shifts from an antiviral to a proviral function: it is redirected on the vRNA, where, isolated from its NMD partner UPF2, it stimulates vRNA export and viral particles maturation (Figure 8).

Methods:

Mutagenesis. To construct Rex mutant plasmids, directed mutagenesis was carried out as follow: a 20 cycles PCR was done with Phusion polymerase, 2µM of complementary primers with the point mutation and 50ng of the parental plasmid (pCMV Rex WT). PCR products were digested by *DpnI* before XL1 blue transformation. For the molecular clone mutagenesis : pCMVHTLV WT and Tax9Q plasmids were already described[70]. To modify Rex, a 1kb fragment between both *BlpI* restriction sites was amplified: the 5' forward primer harboured the nonsense mutation L23stop in the Rex sequence. It is neutral for the Tax sequence encoded on the same RNA. The DNA fragment and retroviral backbone were digested by *BlpI* (NEB). Both were ligated at 16°C overnight with T4 DNA ligase (NEB) before XL1 blue transformation. All mutants were validated by Sanger sequencing (Genewiz). See supplementary method for all the primer sequences.

Immunoprecipitations. ~2 × 10^6 293T cells were transfected as described in the figures using jet prime reagent (Polyplus). 48h post transfection, cells were washed with PBS two times and pelleted in two dry pellets: 10% of the cells were put aside and directly resuspended in Laemmli buffer (loading buffer). It is referred as the INPUT fraction. The other pellet composed of the remaining 90% cells was resuspended in 400µl of lysis buffer (50 mM Tris–Cl, pH 8, 1% Triton, 10% glycerol, 0.05% SDS, 0.1 mM EDTA, 0.1 mM GTP, 200 mM KCl, protease inhibitor (Roche)) for 30 min at 4°C. The soluble fraction obtained after centrifugation at 11,000g for 10 min was pre-cleared with sepharose beads pre-coated with tRNA and BSA-0.3% for 30 min. Supernatant was further incubated with primary antibody (5 µl) overnight at 4 °C. Protein A Sepharose® beads (Sigma) were coated with PBS + 0.3% BSA, supplemented with tRNA overnight. After re-equilibration in lysis buffer, 30 µl of beads were added to the lysate for 2h30 at 4°C before three extensive washings of 15 min in lysis buffer. The dry beads were resuspended in loading buffer for western blotting. For RNase treatment, 0.1 mg/ml RNAse A was added before the washing step.

Immunofluorescence. 50000 cells were cultivated per well into 4 well Chamber Slide™ Labtek® II in DMEM (for HeLa or 293T cells) or RPMI medium (for Jurkat, C91PL or C8166 cells) complemented with 10% SVF and Penicillin/Streptomycin. 48h after transfection (HeLa or 293T) or after 30 minutes of sedimentation at room temperature (Jurkat, C91PL, C8166 cells), cells were fixed with 4% PFA during 20 min. After extensive washing, aldehyde groups were saturated in a 0.1M PBS Glycine solution for 30 min then washed one time with PBS 1X. Cells were permeabilized with PBS-1%Triton for 5 min and then extensively washed. Saturation of non-specific sites was performed by 0.1% BSA-PBS for 30 min then extensively washed. The indicated primary antibodies were incubated for 1h30 at Room Temperature (RT) at 1/1000 (vol/vol) and further washed three times. Secondary antibodies were incubated for 50 min at 1/500 before three washes. Hoechst coloration was used to visualized nucleus (1 ng/ml final concentration). Fluoromount-G® from SouthernBiotech was used before recovering with cover slips 22*60 mm from Menzel Gläser.

Proximity Ligation Assay (PLA). HA Rex plasmid was transfected in 293T cells using jet Optimus. After 24h, cells were subjected to PLA using a kit and following the manufacturer indications. Dilutions of primary antibodies (vol/vol): anti-UPF1 (1/250eme) ; anti-AKT1 (1/50eme) ; anti-HA (1/500eme) ; anti-FTSJ1 (1/250eme) ; anti-eIF4E (1/250eme) ; anti-eIF5A (1/250eme). Dilutions of secondary antibodies (PLUS and MINUS): 1/5eme. Acquisition were performed with Spinning Disk at 60x oil objective (Live SR) microscope. Huygens

Professional software was used for image deconvolution. ImageJ software was used to image treatment and IMARIS software to count based on 8 pictures per condition. Experiment was repeated twice.

Image acquisition, treatment and manual counting. Image acquisitions were performed with the confocal microscope LSM800 at 63x oil objective. ImageJ software (Fiji Version 2.3.0) was used to apply 'gaussian blur' filter (3.00 rad) to all images. Then colocalization pixel was performed on 8-bit gray scale images with the function "image calculator" and "AND" command between channels of interest. Gray scale was used to identify common pixels. For UPF1 nuclear retention quantification, common pixels between UPF1 and nucleus was used to determine the proportion of nuclear UPF1 with a yes or no criteria. The detection of cytoplasmic and nucleus region of interest (ROI) was determined on the signal strength from UPF1+CRM1 channels and Hoechst+CRM1 channels respectively, then manually verified and/or adjusted. To avoid bias from disparate volumes and proximity of different cells, ROI cytoplasm was restricted to an area near the nuclear ROI. Then, nuclear/cytoplasmic ratio was extracted from fluorescence intensity mean in each ROI. For foci identification, the detouring of CRM1 signals was performed with ImageJ too, then UPF1 colocalization was determined based on colocalization pixel function and extracted with a Yes or No criteria. n = 54 for control, n = 36 for Rex, n = 37 for Rev, n = 67 for C91PL and n = 66 for C8166 conditions. P values were calculated by performing first Fischer test then a Student's t-test (paired, two-tailed) ns: $P > 0.05$; $*P < 0.05$; $**P < 0.01$.

RNA immunoprecipitation (RIP). ~6×10^6 HeLa cells were transfected as described in the figures, harvested and resuspended in lysis buffer (50mM Tris–Cl, pH 7.5, 1% NP-40, 0.5% sodium deoxycholate, 0.05% SDS, 1mM EDTA, 150mM NaCl, protease inhibitor (Roche) and RNAsin (Promega)) as previously described[41]. Extracts obtained after centrifugation at 12000g for 15 min were separated in 2: 10% is the input fraction and the 90% remaining are incubated with primary antibody overnight at 4 °C for immunoprecipiation. Protein A and G magnetic beads (Dynabeads, Life Technology; 5 µl each) were mixed and coated with PBS + 0.3% BSA, supplemented with tRNA and RNasin (Promega) overnight. After re-equilibration in lysis buffer (supplemented with tRNA), the beads were added to the lysate for 2h at 4°C before extensive washing in lysis buffer. The beads were resuspended in elution buffer (50mM Tris–HCl, pH 7, 0.1mM EDTA, 10mM DTT and 1% SDS).

Double RIP were performed as reported previously[41]: ~ 18×10^6 HeLa cells were transfected as described in the figures, harvested and fixed with 0.05% formaldehyde for 20 min at room temperature. Then, 0.25M glycine was added for 5min before PBS washing. The cell pellet was resuspended in lysis buffer, and the lysate was sonicated (Bioruptor, diagenode). First, the HA tag was immunoprecipitated. The immunoprecipitation steps were carried out as described for simple RIP except that samples were incubated with Sepharose beads. Extensive washings were performed with 50mM Tris–Cl, pH 7.5, 1% NP-40, 0.5% sodium deoxycholate, 0.05% SDS, 1mM EDTA, 1M NaCl and 1M urea. The beads were resuspended in elution buffer (50mM Tris–Cl, pH 8, 1% Triton, 10% glycerol, 0.05% SDS, 0.1mM EDTA, 0.1mM GTP, 200mM KCl, protease inhibitor (Roche), RNAsin + HA peptide at 0.1 mg/ml) and incubated at 4°C for 1h, then for 10min at 30°C to ensure elution. Finally, the elution volume was increased to 400µl and Rex immunoprecipitation was performed. After extensive washing, the formaldehyde fixation was reversed by heating samples 45min at 70°C.

For all RIP experiments, the beads and the input fraction were treated with 1ml of RNAzol RT reagent for RNA extraction. RNA was quantified by qRT-PCR using the indicated

primers. The levels of immunoprecipitated RNA are expressed as % input. The values represented in the graphs correspond to the mean of at least three biological replicates, and the error bars correspond to the SEM. P values were calculated by performing a Student's t-test (unpaired, two-tailed) ns: $P > 0.05$; *$P < 0.05$; **$P < 0.01$.; ***$P< 0.005$. See supplementary method for all the primer sequences.

RNA decay assays and qRT-PCR/RT-PCR. RNA decay assays were performed to assess the stability of mRNA expressed from a β-globin reporter minigene that was either WT (GlobinWT) or with a PTC in the second exon (GlobinPTC). For this procedure, 0.5µg of GlobinPTC or 0.05µg of GlobinWT constructs were co-transfected as indicated with 0.5µg of renilla-expressing vector (unsensitive to NMD) in 0.7×10^6 HeLa cells with jet prime reagent (Polyplus). Additional plasmids were co-transfected as indicated in the figures. After 48h, the cells were treated with DRB (100µg.ml^{-1}) to block transcription for 0, 1, 3 or 4 h. Total mRNAs were extracted using the Macherey-Nagel RNA easy extraction kit and quantified by qRT-PCR using the QuantiTect SYBR Green qRT-PCR kit (Qiagen) and appropriate primers. The values represented in the graphs correspond to the mean of at least three biological replicates, and the error bars correspond to the SEM. Half-lives were calculated for each replicate, and P values were calculated by performing a Student's t-test (unpaired, two-tailed) ns: $P > 0.05$; *$P < 0.05$; **$P < 0.01$.

Viral transmission assay. Viral transmission assay were performed as previously described [57,71] with the following modifications : $0.2\text{x}10^6$ C91PL were infected at J0 for 24h with lentivirus expressing shRNA against UPF1 or a Control (Dharmacon) at MOI =1 in 1ml of RPMI. J4: shRNA expression was induced with doxycycline treatment (0.5µg/ml). To ensure a maximum of viral biofilm renewal in the absence of UPF1, a second dose of doxycycline treatment was applied at J7. At J10, C91PL were counted: $0.05\text{x}10^6$ cells were co-cultured with $0.15\text{x}10^6$ Jurkat cells engineered to stably express luciferase under the control of a HTLV-1 LTR promoter (selection with 450ng/ml hygromycin). In parallel, remaining C91PL were analysed by FACS to monitor extracellular levels of ENV, indicative of surface-bound viral particles levels (viral biofilm). After 24h of co-culture (J11), cells were treated for Luciferase assay, following the manufacturer protocol (Promega). Luciferase values were normalized by the corresponding ENV levels, previously quantified. This normalization was possible since we identified that ENV levels were weakly affected by UPF1 knock down. The graphs represent the mean of at least 3 independent viral transmissions with SD.

Preparation of viral samples for proteomic studies: CEM T cells (as a non-infected control) and HTLV-1-infected T cell line C91PL were from the NIH AIDS Research and Reference Reagent Program. Viral preparations were obtained from cultures ($5\text{x}10^5$cells/ml) grown for 3 days.

Free particles samples preparation: Supernatants (30ml) were clarified by centrifugation (5 min at 800g) and filtered through a 0.2µm diameter pore filter (Millipore, MA) to remove cell debris and the viral biofilms potentially detached from cultured cells. Individual cell-free virions were then purified by ultracentrifugation through a 20% sucrose (wt/vol in PBS) cushion at 83,000 g in an SW41 rotor (Beckman) for 2 h min at 4°C. Viral pellets were resuspended in serum-free RPMI 1640 medium to obtain a 500-fold concentrated suspension of individual cell-free viral particles.

Extracellular fraction samples (ECF) preparation: preparations ECF was carried out as described previously[57], with minor modifications. Briefly, C91PL and CEM cells were washed 2 times in serum-free RPMI 1640 medium before being concentrated 3 times in

serum-free RPMI 1640 medium (10 ml). Cell suspensions were then gently vortexed with a gentleMACS™ Dissociator (Miltenyi Biotech). The cells were pelleted by centrifugation and supernatants containing the ECF were collected. ECF were purified by ultracentrifugation through a 20% sucrose (wt/vol in PBS) cushion at 38,500g in an SW41 rotor (Beckman) for 1 h min at 4°C. ECF pellets were then resuspended in RPMI 1640 serum-free medium.

Three independent replicates were performed for each sample type. Prior to processing for proteomic studies, infectivity of samples was inactivated by heating at 85°C for 30 minutes in the presence of 0.5% SDS and 10mM Hepes.

Mass spectrometry analysis

Samples were vortexed in 1% IgePal (Merck) and digested ON with PGNase F (Merck) before solubilization in 8M urea and 50 mM Tris, pH 8.0. Proteins were reduced with 5 mM TCEP for 30 minutes at room temperature, followed by alkylation with 20 mM IAM for 30 minutes in the dark. The urea concentration was reduced below 2M with 50 mM ammonium bicarbonate. Digestion was performed first with Endoprotease LysC (Promega) and then with trypsin (ratio of 1:50) at 37°C for 3 hours and overnight, respectively. The digestion was stopped with 1% formic acid (FA) before desalting using a C18 SepPak column (Waters). The eluted peptides were dried and resuspended in 0.1% FA before injection

LC-MS/MS analysis of the digested peptides was conducted using an Orbitrap Q Exactive Plus mass spectrometer coupled to an EASY-nLC 1200 (Thermo Fisher Scientific). A *home-made* column (C18 50 cm capillary column picotip silica emitter tip (75 µm diameter) filled with 1.9 µm Reprosil-Pur Basic C18-HD resin, Dr. Maisch GmbH, Ammerbuch-Entringen, Germany) was used for peptide separation. Peptides were loaded in 0.1% FA at 900 bars and separated at 250 nl/min using a gradient of ACN, 0.1% FA, with a step-wise increase from 3% to 7% over 8 minutes, 7% to 23% over 95 minutes, and 23% to 45% over 45 minutes (total chromatographic run time of 170 minutes, including a high ACN level step and column regeneration).

Mass spectra were acquired in data-dependent acquisition mode using the XCalibur 2.2 software with automatic switching between MS and MS/MS scans using a top 12 method. MS spectra were acquired at a resolution of 35,000 at m/z 400 with a target value of 3×10^6 ions. The scan range was limited from 300 to 1700 m/z. Peptide fragmentation was performed using higher-energy collision dissociation with an energy setting of 27 NCE. The intensity threshold for ion selection was set at 1×10^6 ions with charge exclusion for $z = 1$ and $z > 7$. The MS/MS spectra were acquired at a resolution of 17,500 at m/z 400, and the isolation window was set at 1.6 Th. Dynamic exclusion was employed within 45 seconds.

Data analysis was conducted using MaxQuant (version 2.1.4.0) with the Andromeda search engine [72,73] against a reference proteome of Human 9606 (22811 entries, downloaded from UniProt on May 10th, 2023) and HTLV downloaded from uniprot). The following search parameters were applied: carbamidomethylation of cysteines was set as a fixed modification, oxidation of methionine and protein N-terminal acetylation were set as variable modifications. The mass tolerances in MS and MS/MS were set to 5 ppm and 20 ppm respectively. Maximum peptide charge was set to 7 and 5 amino acids were required as minimum peptide length. A false discovery rate of 1% was set up for both protein and peptide levels. The iBAQ intensity was used to estimate the protein abundance within a sample. The match between runs features was allowed.

References

1. Okamura, M., Inose, H. & Masuda, S. RNA Export through the NPC in Eukaryotes. *Genes* **6**, 124–149 (2015).
2. Cautain, B., Hill, R., de Pedro, N. & Link, W. Components and regulation of nuclear transport processes. *FEBS J.* **282**, 445–462 (2015).
3. Fung, H. Y. J., Niesman, A. & Chook, Y. M. An update to the CRM1 cargo/NES database NESdb. *Mol. Biol. Cell* **32**, 467–469 (2021).
4. Fung, H. Y. J. & Chook, Y. M. Atomic basis of CRM1-cargo recognition, release and inhibition. *Semin. Cancer Biol.* **27**, 52–61 (2014).
5. Güttler, T. & Görlich, D. Ran-dependent nuclear export mediators: a structural perspective. *EMBO J.* **30**, 3457–3474 (2011).
6. Güttler, T. *et al.* NES consensus redefined by structures of PKI-type and Rev-type nuclear export signals bound to CRM1. *Nat. Struct. Mol. Biol.* **17**, 1367–1376 (2010).
7. Kehlenbach, R. H., Dickmanns, A. & Gerace, L. Nucleocytoplasmic shuttling factors including Ran and CRM1 mediate nuclear export of NFAT In vitro. *J. Cell Biol.* **141**, 863–874 (1998).
8. Fu, S.-C., Fung, H. Y. J., Cağatay, T., Baumhardt, J. & Chook, Y. M. Correlation of CRM1-NES affinity with nuclear export activity. *Mol. Biol. Cell* **29**, 2037–2044 (2018).
9. Engelsma, D., Bernad, R., Calafat, J. & Fornerod, M. Supraphysiological nuclear export signals bind CRM1 independently of RanGTP and arrest at Nup358. *EMBO J.* **23**, 3643–3652 (2004).
10. Zhang, X., Yamada, M., Mabuchi, N. & Shida, H. Cellular requirements for CRM1 import and export. *J. Biochem. (Tokyo)* **134**, 759–764 (2003).
11. Hill, R., Cautain, B., de Pedro, N. & Link, W. Targeting nucleocytoplasmic transport in cancer therapy. *Oncotarget* **5**, 11–28 (2014).
12. Nguyen, K. T., Holloway, M. P. & Altura, R. A. The CRM1 nuclear export protein in normal development and disease. *Int. J. Biochem. Mol. Biol.* **3**, 137–151 (2012).
13. Saulino, D. M., Younes, P. S., Bailey, J. M. & Younes, M. CRM1/XPO1 expression in pancreatic adenocarcinoma correlates with survivin expression and the proliferative activity. *Oncotarget* **9**, 21289–21295 (2018).
14. Chen, Y. *et al.* Inhibition of the Nuclear Export Receptor XPO1 as a Therapeutic Target for Platinum-Resistant Ovarian Cancer. *Clin. Cancer Res. Off. J. Am. Assoc. Cancer Res.* **23**, 1552–1563 (2017).
15. Jiang, Y. *et al.* Circ-XPO1 upregulates XPO1 expression by sponging multiple miRNAs to facilitate osteosarcoma cell progression. *Exp. Mol. Pathol.* **117**, 104553 (2020).
16. Song, P., Li, W., Xie, J., Hou, Y. & You, C. Cytokine storm induced by SARS-CoV-2. *Clin. Chim. Acta Int. J. Clin. Chem.* **509**, 280–287 (2020).
17. Ferreira, B. I., Cautain, B., Grenho, I. & Link, W. Small Molecule Inhibitors of CRM1. *Front. Pharmacol.* **11**, 625 (2020).
18. Wang, A. Y. & Liu, H. The past, present, and future of CRM1/XPO1 inhibitors. *Stem Cell Investig.* **6**, 6 (2019).
19. Kırlı, K. *et al.* A deep proteomics perspective on CRM1-mediated nuclear export and nucleocytoplasmic partitioning. *eLife* **4**, e11466 (2015).
20. Thakar, K., Karaca, S., Port, S. A., Urlaub, H. & Kehlenbach, R. H. Identification of CRM1-dependent Nuclear Export Cargos Using Quantitative Mass Spectrometry. *Mol. Cell. Proteomics MCP* **12**, 664–678 (2013).
21. Mendell, J. T., Sharifi, N. A., Meyers, J. L., Martinez-Murillo, F. & Dietz, H. C. Nonsense surveillance regulates expression of diverse classes of mammalian transcripts and mutes genomic noise. *Nat Genet* **36**, 1073–8 (2004).
22. Lejeune, F. Nonsense-Mediated mRNA Decay, a Finely Regulated Mechanism. *Biomedicines* **10**, 141 (2022).
23. Hurt, J. A., Robertson, A. D. & Burge, C. B. Global analyses of UPF1 binding and function reveal expanded scope of nonsense-mediated mRNA decay. *Genome Res* **23**, 1636–1650 (2013).
24. Zund, D., Gruber, A. R., Zavolan, M. & Muhlemann, O. Translation-dependent displacement of UPF1 from coding sequences causes its enrichment in 3' UTRs. *Nat Struct Mol Biol* **20**, 936–43 (2013).
25. Neu-Yilik, G. *et al.* Dual function of UPF3B in early and late translation termination. *EMBO J.* **36**, 2968–2986 (2017).
26. Chamieh, H., Ballut, L., Bonneau, F. & Le Hir, H. NMD factors UPF2 and UPF3 bridge UPF1 to the exon junction complex and stimulate its RNA helicase activity. *Nat Struct Mol Biol* **15**, 85–93 (2008).
27. Yamashita, A., Ohnishi, T., Kashima, I., Taya, Y. & Ohno, S. Human SMG-1, a novel phosphatidylinositol 3-kinase-related protein kinase, associates with components of the mRNA surveillance complex and is involved in the regulation of nonsense-mediated mRNA decay. *Genes Dev* **15**, 2215–28 (2001).
28. Palma, M. *et al.* A role for AKT1 in nonsense-mediated mRNA decay. *Nucleic Acids Res.* **49**, 11022–11037 (2021).

29. Cho, H. *et al.* AKT constitutes a signal-promoted alternative exon-junction complex that regulates nonsense-mediated mRNA decay. *Mol. Cell* **82**, 2779-2796.e10 (2022).
30. Durand, S., Franks, T. M. & Lykke-Andersen, J. Hyperphosphorylation amplifies UPF1 activity to resolve stalls in nonsense-mediated mRNA decay. *Nat. Commun.* **7**, 12434 (2016).
31. Balistreri, G. *et al.* The host nonsense-mediated mRNA decay pathway restricts Mammalian RNA virus replication. *Cell Host Microbe* **16**, 403–411 (2014).
32. Hogg, J. R. & Goff, S. P. Upf1 senses 3'UTR length to potentiate mRNA decay. *Cell* **143**, 379–89 (2010).
33. LeBlanc, J. J. & Beemon, K. L. Unspliced Rous sarcoma virus genomic RNAs are translated and subjected to nonsense-mediated mRNA decay before packaging. *J. Virol.* **78**, 5139–5146 (2004).
34. Wada, M., Lokugamage, K. G., Nakagawa, K., Narayanan, K. & Makino, S. Interplay between coronavirus, a cytoplasmic RNA virus, and nonsense-mediated mRNA decay pathway. *Proc. Natl. Acad. Sci. U. S. A.* **115**, E10157–E10166 (2018).
35. Quek, B. L. & Beemon, K. Retroviral strategy to stabilize viral RNA. *Curr. Opin. Microbiol.* **18**, 78–82 (2014).
36. Garcia, D., Garcia, S. & Voinnet, O. Nonsense-mediated decay serves as a general viral restriction mechanism in plants. *Cell Host Microbe* **16**, 391–402 (2014).
37. Li, M. *et al.* Identification of antiviral roles for the exon-junction complex and nonsense-mediated decay in flaviviral infection. *Nat. Microbiol.* **4**, 985–995 (2019).
38. Mocquet, V. *et al.* The human T-lymphotropic virus type 1 tax protein inhibits nonsense-mediated mRNA decay by interacting with INT6/EIF3E and UPF1. *J Virol* **86**, 7530–43 (2012).
39. Nakano, K. *et al.* Viral interference with host mRNA surveillance, the nonsense-mediated mRNA decay (NMD) pathway, through a new function of HTLV-1 Rex: implications for retroviral replication. *Microbes Infect.* **15**, 491–505 (2013).
40. Popp, M. W.-L., Cho, H. & Maquat, L. E. Viral subversion of nonsense-mediated mRNA decay. *RNA N. Y. N* **26**, 1509–1518 (2020).
41. Fiorini, F. *et al.* HTLV-1 Tax plugs and freezes UPF1 helicase leading to nonsense-mediated mRNA decay inhibition. *Nat. Commun.* **9**, (2018).
42. Nakano, K. *et al.* Elucidation of the Mechanism of Host NMD Suppression by HTLV-1 Rex: Dissection of Rex to Identify the NMD Inhibitory Domain. *Viruses* **14**, 344 (2022).
43. Bogerd, H. P., Echarri, A., Ross, T. M. & Cullen, B. R. Inhibition of human immunodeficiency virus Rev and human T-cell leukemia virus Rex function, but not Mason-Pfizer monkey virus constitutive transport element activity, by a mutant human nucleoporin targeted to Crm1. *J. Virol.* **72**, 8627–8635 (1998).
44. Shida, H. Role of Nucleocytoplasmic RNA Transport during the Life Cycle of Retroviruses. *Front. Microbiol.* **3**, 179 (2012).
45. Nakano, K. & Watanabe, T. HTLV-1 Rex: the courier of viral messages making use of the host vehicle. *Front. Microbiol.* **3**, 330 (2012).
46. Ahmed, Y. F., Hanly, S. M., Malim, M. H., Cullen, B. R. & Greene, W. C. Structure-function analyses of the HTLV-I Rex and HIV-1 Rev RNA response elements: insights into the mechanism of Rex and Rev action. *Genes Dev.* **4**, 1014–1022 (1990).
47. Palmeri, D. & Malim, M. H. Importin beta can mediate the nuclear import of an arginine-rich nuclear localization signal in the absence of importin alpha. *Mol. Cell. Biol.* **19**, 1218–1225 (1999).
48. Ballaun, C. *et al.* Functional analysis of human T-cell leukemia virus type I rex-response element: direct RNA binding of Rex protein correlates with in vivo activity. *J. Virol.* **65**, 4408–4413 (1991).
49. Hakata, Y., Umemoto, T., Matsushita, S. & Shida, H. Involvement of human CRM1 (exportin 1) in the export and multimerization of the Rex protein of human T-cell leukemia virus type 1. *J. Virol.* **72**, 6602–6607 (1998).
50. Nakano, K. & Watanabe, T. HTLV-1 Rex Tunes the Cellular Environment Favorable for Viral Replication. *Viruses* **8**, 58 (2016).
51. Kress, E., Baydoun, H. H., Bex, F., Gazzolo, L. & Duc Dodon, M. Critical role of hnRNP A1 in HTLV-1 replication in human transformed T lymphocytes. *Retrovirology* **2**, 8 (2005).
52. Thermann, R. *et al.* Binary specification of nonsense codons by splicing and cytoplasmic translation. *Embo J* **17**, 3484–94 (1998).
53. Behrens, R. T., Aligeti, M., Pocock, G. M., Higgins, C. A. & Sherer, N. M. Nuclear Export Signal Masking Regulates HIV-1 Rev Trafficking and Viral RNA Nuclear Export. *J. Virol.* **91**, e02107-16 (2017).
54. Ajamian, L. *et al.* HIV-1 Recruits UPF1 but Excludes UPF2 to Promote Nucleocytoplasmic Export of the Genomic RNA. *Biomolecules* **5**, 2808–2839 (2015).
55. Liu, B., Hong, S., Tang, Z., Yu, H. & Giam, C.-Z. HTLV-I Tax directly binds the Cdc20-associated anaphase-promoting complex and activates it ahead of schedule. *Proc. Natl. Acad. Sci. U. S. A.* **102**, 63–68 (2005).
56. Baydoun, H. H., Bellon, M. & Nicot, C. HTLV-1 Yin and Yang: Rex and p30 master regulators of viral mRNA trafficking. *AIDS Rev.* **10**, 195–204 (2008).

57. Pais-Correia, A.-M. *et al.* Biofilm-like extracellular viral assemblies mediate HTLV-1 cell-to-cell transmission at virological synapses. *Nat. Med.* **16**, 83–89 (2010).
58. Alais, S., Mahieux, R. & Dutartre, H. Viral Source-Independent High Susceptibility of Dendritic Cells to Human T-Cell Leukemia Virus Type 1 Infection Compared to That of T Lymphocytes. *J. Virol.* **89**, 10580–10590 (2015).
59. Soo, C. Y. *et al.* Nanoparticle tracking analysis monitors microvesicle and exosome secretion from immune cells: Nanoparticle tracking analysis of microvesicles and exosomes. *Immunology* **136**, 192–197 (2012).
60. Liu, Y.-J. & Wang, C. A review of the regulatory mechanisms of extracellular vesicles-mediated intercellular communication. *Cell Commun. Signal. CCS* **21**, 77 (2023).
61. Singh, A. K. *et al.* The RNA helicase UPF1 associates with mRNAs co-transcriptionally and is required for the release of mRNAs from gene loci. *eLife* **8**, e41444 (2019).
62. Nakano, K. *et al.* Exploring New Functional Aspects of HTLV-1 RNA-Binding Protein Rex: How Does Rex Control Viral Replication? *Viruses* **14**, 407 (2022).
63. Ajamian, L. *et al.* Unexpected roles for UPF1 in HIV-1 RNA metabolism and translation. *RNA N. Y. N* **14**, 914–927 (2008).
64. Serquina, A. K. *et al.* UPF1 Is Crucial for the Infectivity of Human Immunodeficiency Virus Type 1 Progeny Virions. *J Virol* **87**, 8853–61 (2013).
65. King, J. A., Dubielzig, R., Grimm, D. & Kleinschmidt, J. A. DNA helicase-mediated packaging of adeno-associated virus type 2 genomes into preformed capsids. *EMBO J.* **20**, 3282–3291 (2001).
66. Patkar, C. G. & Kuhn, R. J. Yellow Fever virus NS3 plays an essential role in virus assembly independent of its known enzymatic functions. *J. Virol.* **82**, 3342–3352 (2008).
67. Yu, S. F., Lujan, P., Jackson, D. L., Emerman, M. & Linial, M. L. The DEAD-box RNA Helicase DDX6 is Required for Efficient Encapsidation of a Retroviral Genome. *PLoS Pathog.* **7**, e1002303 (2011).
68. Ma, J. *et al.* The requirement of the DEAD-box protein DDX24 for the packaging of human immunodeficiency virus type 1 RNA. *Virology* **375**, 253–264 (2008).
69. Hu, J., Li, P., Shi, B. & Tie, J. Importin β1 mediates nuclear import of the factors associated with nonsense-mediated RNA decay. *Biochem. Biophys. Res. Commun.* **542**, 34–39 (2021).
70. Mazurov, D., Ilinskaya, A., Heidecker, G., Lloyd, P. & Derse, D. Quantitative comparison of HTLV-1 and HIV-1 cell-to-cell infection with new replication dependent vectors. *PLoS Pathog.* **6**, e1000788 (2010).
71. Cachat, A. *et al.* ADAR1 enhances HTLV-1 and HTLV-2 replication through inhibition of PKR activity. *Retrovirology* **11**, 93 (2014).
72. Cox, J. *et al.* Andromeda: a peptide search engine integrated into the MaxQuant environment. *J. Proteome Res.* **10**, 1794–1805 (2011).
73. Tyanova, S., Temu, T. & Cox, J. The MaxQuant computational platform for mass spectrometry-based shotgun proteomics. *Nat. Protoc.* **11**, 2301–2319 (2016).

Author Contributions: All authors have read and agreed to publish this version of the manuscript.
Experimentation and Analysis, L.P., M.MH, A.R., M.P., JP.R., L.S., S.D., D.C., M.M., D.D, M.M., S.R., A.D. and V.M. Conceptualization, V.M.; writing, L.P., M.MH., H.D., MI T., F.L., P.J. and V.M.; funding acquisition, L.P. and V.M.

Acknowledgments: We would like to thank Derse's lab for the pCMV-HTLV-1 plasmids and A. Gessain for anti HTLV-1 serum. We also thank S. Alais for technical support with ELISA and the harvest of lymphocytes extracellular matrix, P. Solanes for help in setting up the proteomic study, F. Mortreux, C. Pique and C. Journo for useful comments on the manuscript. We acknowledge the contribution of SFR Biosciences (UMS3444/CNRS, US8/Inserm, ENS de Lyon, UCBL) facilities: the PLATIM and especially C. Lionnet and E. Chartre for the assistance with microscopy experiments; the center AniRA from CEPHALIA infrastructure (FACS and vectorology) and especially Gisèle Froment, Didier Nègre and C. Costa.
Work in the authors' laboratory is supported by grants from foundation ARC (V. M.), from La Ligue Isere contre le Cancer (V.M.), from l'Institut Pasteur (PTR-445 : grant (MI.T.) and fellowship (A.D.)) and from French Agence Nationale de Recherche sur le SIDA et les Hépatites Virales (ANRS) (grant (V.M.) and fellowship (L.P.)).

Conflicts of Interest: The authors declare no conflicts of interest. The funders had no role in the design of the study, in the writing of the manuscript, or in the decision to publish the results.

Figures

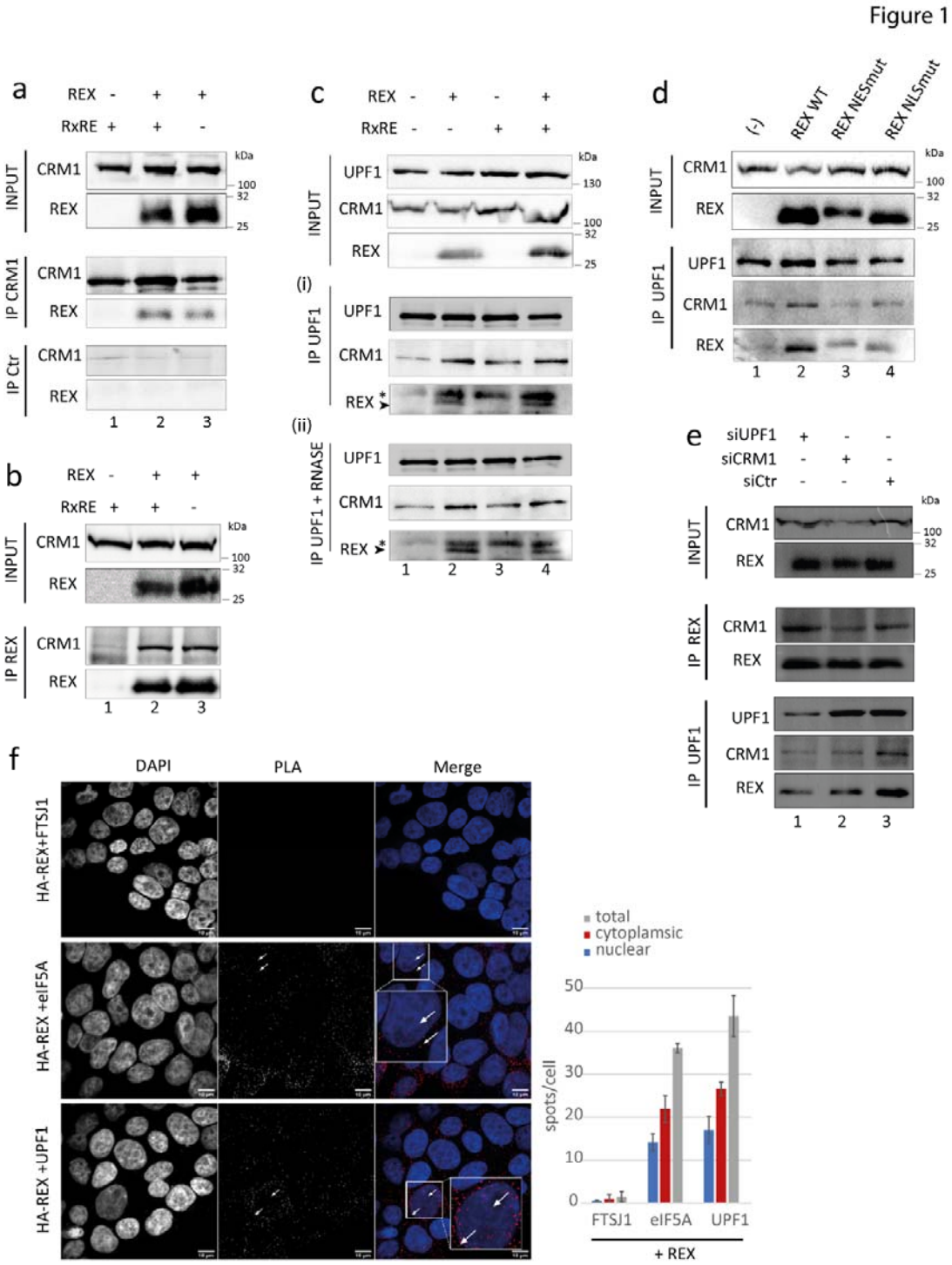

Figure 1: *Rex interacts with CRM1 and UPF1 to form a tripartite complex*.

a) Co-immunoprecipitation (coIP) experiments on 293T cells extracts. Cells express the indicated combinations of Rex and RNA containing the RxRE motif. IP were performed using rabbit polyclonal antibodies against CRM1 (middle panel) or from a pre-immune serum. Proteins revealed by western blot were indicated on the side. b) Same as A with an antibody targeting Rex. c) Same as a) with an antibody targeting UPF1. CoIP were incubated for 30

min with RNAse A (0.1mg/ml) (panel (ii)) or not (panel (i)). * indicates an aspecific signal. Rex specific signal corresponds to the lower band. d) coIP experiments in 293T cells transfected with plasmids coding the indicated forms of Rex and revealed by western blot. An empty vector is transfected in lane 1. IP was performed with a rabbit polyclonal antibody against UPF1. e) coIP experiments in 293T cells transfected with the indicated siRNA and revealed by western blot. IP was performed against Rex (middle panel) or UPF1 (lower panel). IP UPF1 after siUPF1 treatment define background signals of Rex and CRM1. f) Proximity Ligation Assay (PLA) carried out in 293T cells transiently transfected with a HA-REX coding plasmid. PLA combined antibodies specific of the HA tag and FTSJ1, eIF5A or UPF1 were used as indicated. FTSJ1 (ribosomal RNA methyltransferase 1) is a nucleolar protein used as a negative control (no described interaction with Rex). eIF5A, a known partner of Rex, was used as positive control. Each dot corresponds to the colocalization of the indicated protein with a resolution of 40nm. Magnification of one representative cell is framed in the merge. For each condition, the number of spots per cell and their localisation in the cytoplasmic or nuclear compartment are represented in a bar plot on the right. Scale bar: 10µm

Figure 2

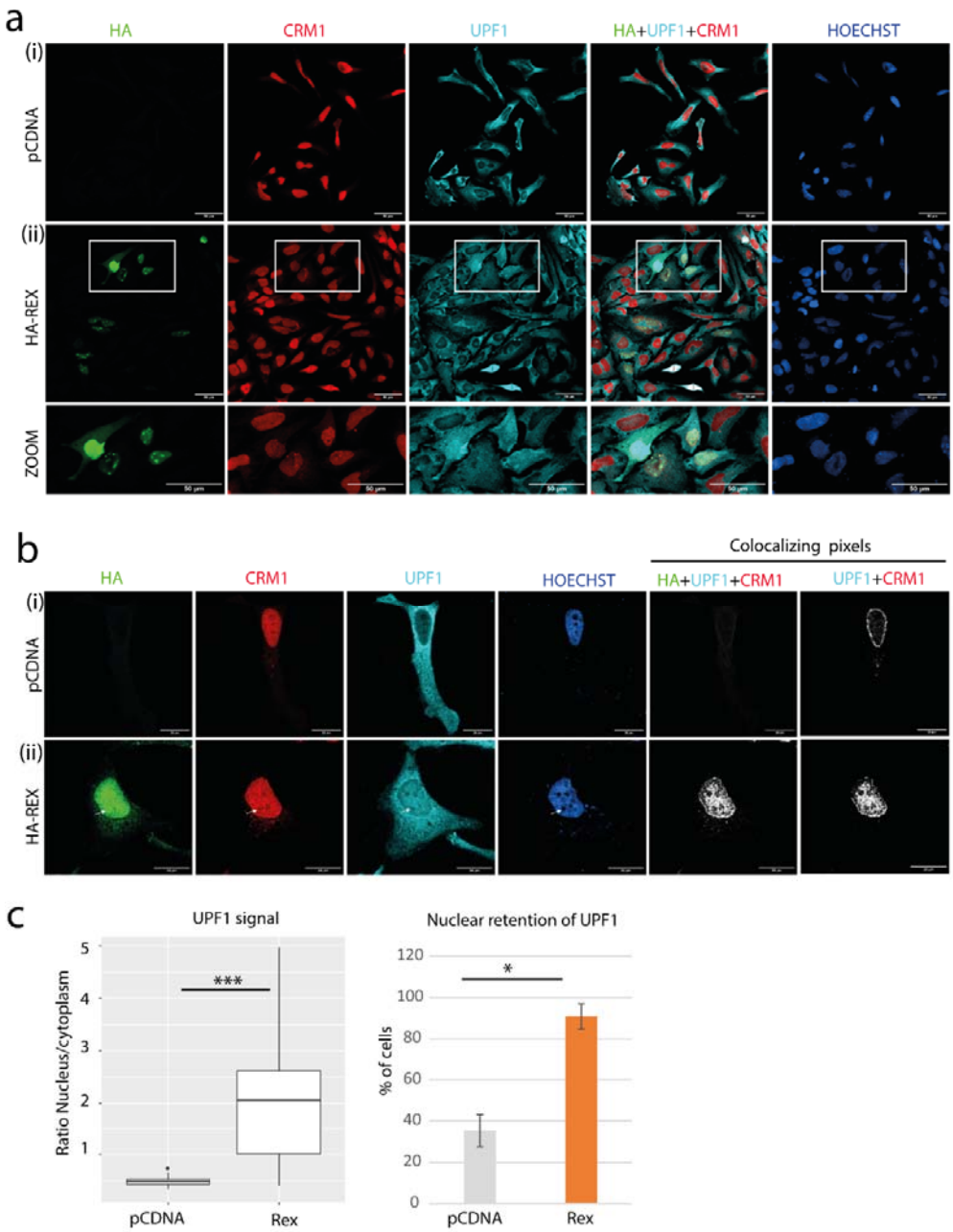

Figure 2 : *Rex expression modifies UPF1 localisation.*

a) Confocal microscopy experiments were performed in HeLa cells transfected with the plasmids indicated on the left side. Rex was revealed with an antiHA tag antibody and an alexa 488 secondary anti mouse. CRM1 antibody was targeted with an alexa 647 anti rabbit and the UPF1 antibody with a CFL 555 anti goat. Magnification of the framed zone is shown in the lower panel (ZOOM). Images were acquired with a x20 objective. Scale bar: 50µm. b) same as A with a x63 objective. Scale bar: 20µm. Colocalizing pixels view is obtained as mentioned in the method section and only show the pixels simultaneously activated with the indicated channels. c) Quantitative analysis of the microscopy experiments. On the left panel, UPF1 signal was quantified in the cytoplasm and in the nucleus and express as a ratio. Wilcoxon, pvalue < 0.005 ***. On the right panel, the number of cells displaying nuclear retention of UPF1 is indicated. Ttest pvalue <0.05 *.

Figure 3

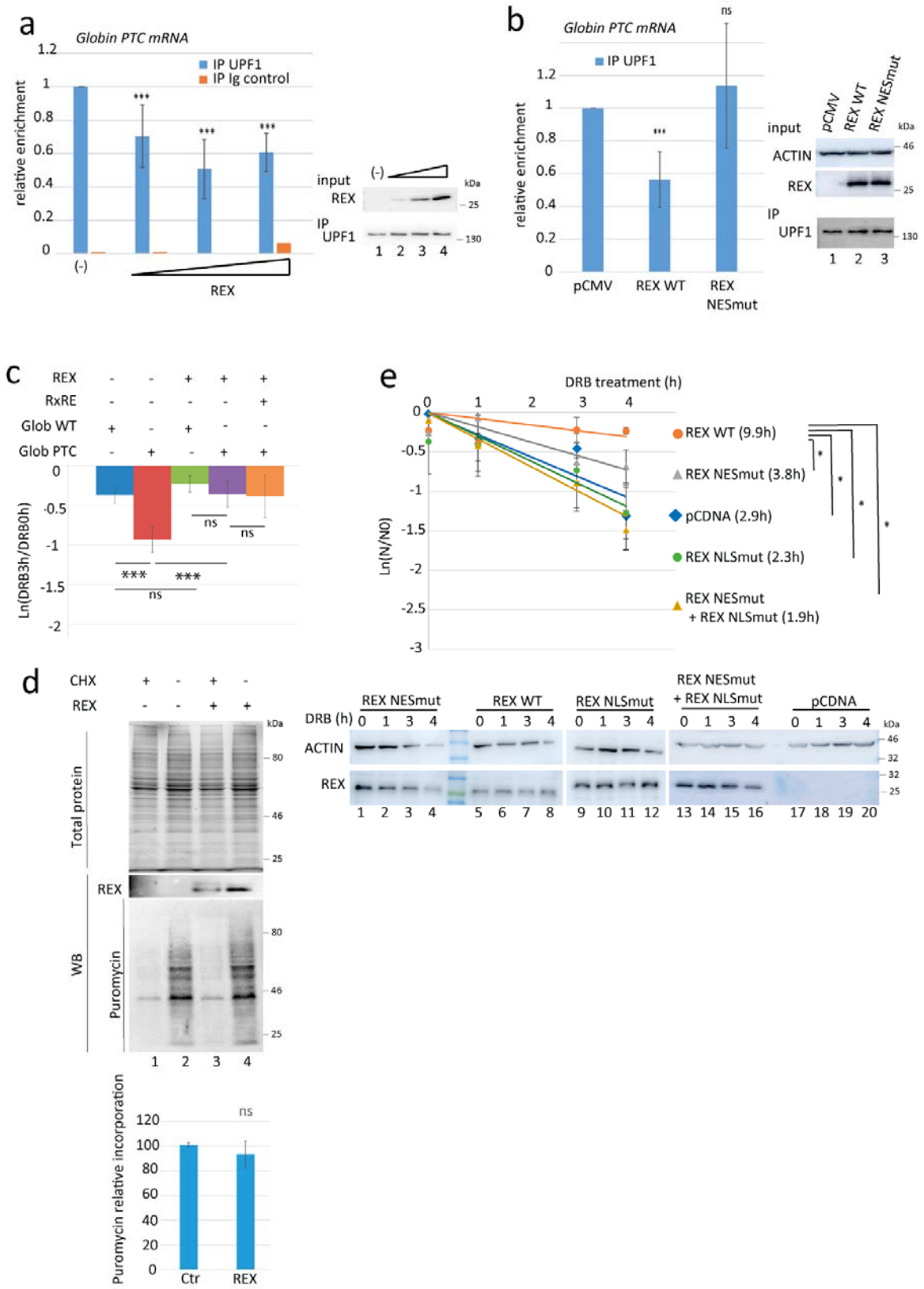
a
Globin PTC mRNA
IP UPF1
IP Ig control
relative enrichment
REX
input
IP
UPF1
b
Globin PTC mRNA
IP UPF1
relative enrichment
pCMV
REX WT
REX NESmut
ACTIN
c
REX
RxRE
Glob WT
Glob PTC
Ln(DRB3h/DRB0h)
d
CHX
Total protein
WB
Puromycin
Puromycin relative incorporation
Ctr
e
DRB treatment (h)
Ln(N/N0)
REX WT (9.9h)
REX NESmut (3.8h)
pCDNA (2.9h)
REX NLSmut (2.3h)
REX NESmut
+ REX NLSmut (1.9h)
DRB (h)

Figure 3: Rex expression leads to UPF1 diminished association to RNA, what is functionally link to NMD inhibition.

a) RNA immunoprecipitation experiment (RIP) using a rabbit polyclonal antibody targeting UPF1 or from a pre-immune serum (Ig control) were performed with HeLa cells transfected with a Globin PTC coding plasmid and increasing amounts of Rex coding plasmid. Immunoprecipitated RNA (Globin PTC) were quantified by RTqPCR. For each condition, the relative enrichment of Globin PTC RNA associated to UPF1 compared to conditions without Rex was displayed in the graph. On the right panel, western blot controlling the levels of the expressed Rex and the immunoprecipitated UPF1. b) Same as A with an empty vector, Rex WT or Rex NES mutant plasmids transfected as indicated. c) Decay rate analysis of Globin PTC and Globin WT RNA. Globin RNA levels were quantified after HeLa cells were treated with DRB for 0h or 3h. The rate of decay is expressed as ln(DRB3h/DRB0h). Statistical analysis is described in the methods section. d) Sunset assay with HeLa cells expressing or not Rex (lane 2 and 4). The level of total protein was acquired before transfer with stainless method, Rex expression and puromycin incorporation were evaluated by western blot. Puromycin quantification was indicated on the right panel. As a negative control, cells were pre-treated with cycloheximid to inhibit translation (lane 1 and 3). Statistical analysis: Ttest ns: $p>0.05$. e) Half-life evaluation of the Glob PTC mRNA in HeLa cells transfected with the indicated forms of Rex. mRNA half-lifes ($t1/2 = \ln(2)/\lambda$ with λ the time constant of the decay curves) are indicated in front of their respective conditions. The expression of Rex at each time point after DRB treatment was evaluated by WB (lower panel).

Figure 4

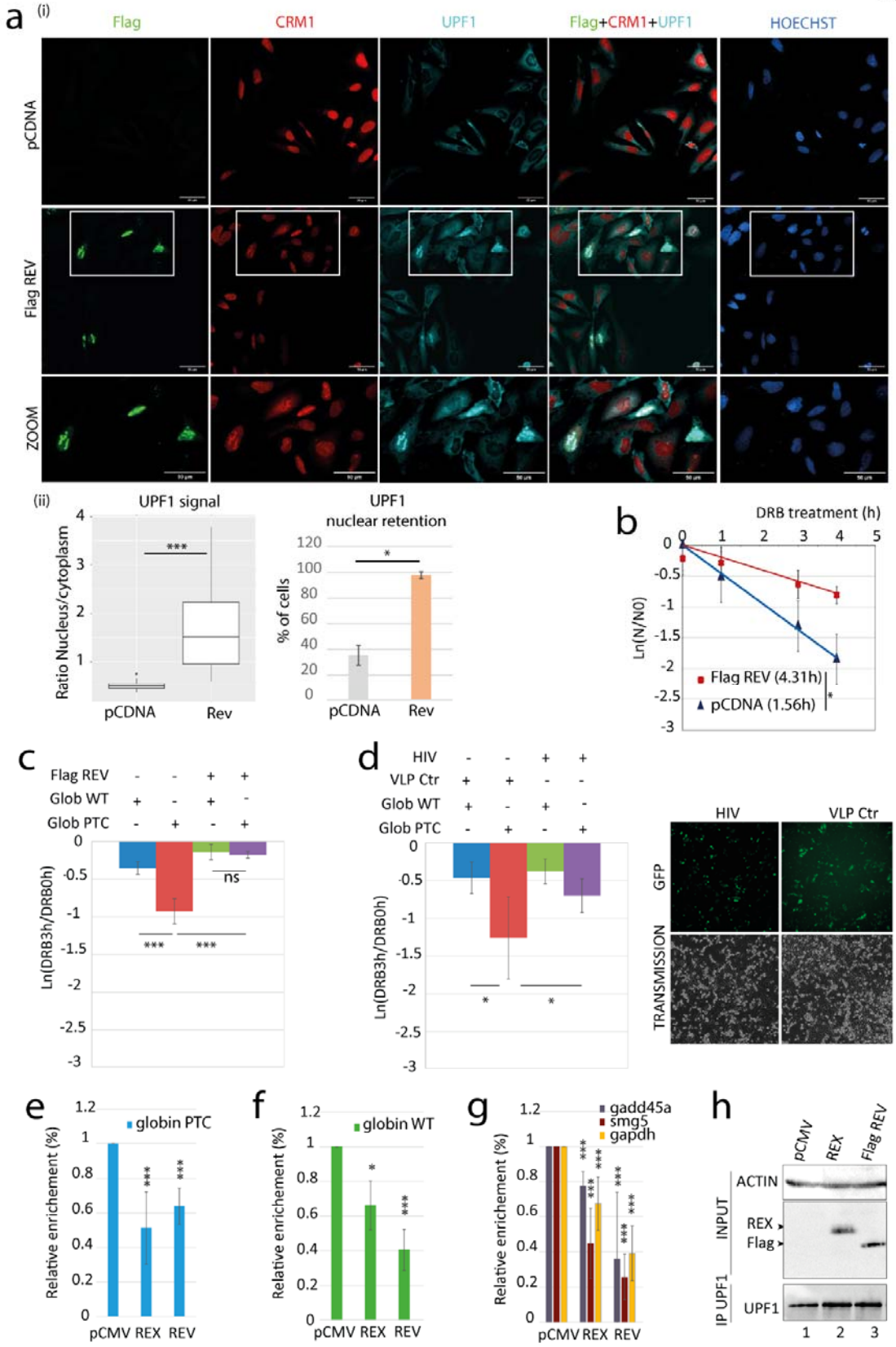
a
(i)
Flag
CRM1
UPF1
Flag+CRM1+UPF1
HOECHST
pCDNA
Flag REV
ZOOM
(ii)
UPF1 signal
Ratio Nucleus/cytoplasm
pCDNA
Rev
UPF1
nuclear retention
% of cells
b
DRB treatment (h)
Ln(N/N0)
Flag REV (4.31h)
pCDNA (1.56h)
c
Flag REV
Glob WT
Glob PTC
Ln(DRB3h/DRB0h)
ns
d
HIV
VLP Ctr
Glob WT
Glob PTC
Ln(DRB3h/DRB0h)
HIV
VLP Ctr
GFP
TRANSMISSION
e
globin PTC
Relative enrichement (%)
pCMV REX REV
f
globin WT
Relative enrichement (%)
pCMV REX REV
g
gadd45a
smg5
gapdh
Relative enrichement (%)
pCMV REX REV
h
pCMV
REX
Flag REV
ACTIN
INPUT
REX
Flag
IP UPF1
UPF1
1 2 3

Figure 4: Rev from HIV-1 also inhibits NMD through UPF1 nuclear retention and diminished RNA association.

a) (i) Confocal microscopy experiments were performed in HeLa cells transfected with the plasmids indicated on the left side. Rev was revealed with an anti Flag tag antibody and an alexa 488 secondary anti-mouse. CRM1 antibody was targeted with an alexa 647 anti-rabbit and the UPF1 antibody with a CFL 555 anti-goat. Magnification of the framed zone is shown in the lower panel (ZOOM). Images were acquired with a x20 objective. Scale bar: 50µm. (ii) The same quantitative analysis was carried out as for Rex in Fig 2C b) Half-life evaluation of the Glob PTC mRNA in HeLa cells transfected with the indicated forms of Rev. mRNA half-life ($t1/2 = \ln(2)/\lambda$ with λ the time constant of the decay curves) are indicated in front of their respective conditions. Statistical analysis: Ttest * $p<0.05$. c) Decay rate analysis of Globin PTC and Globin WT RNA. Globin RNA levels were quantified after HeLa cells were treated with DRB for 0h or 3h. The rate of decay is expressed as ln (DRB3h/DRB0h). Statistical analysis: Ttest *** $p<0.005$; ns: $p>0.05$. d) Same as c) except that HeLa cells were infected with HIV particles or control Virus Like Particles (CtrVLP) instead of being transfected with Flag Rev (left panel). GFP expressed from HIV or CtrVLP was observed with an epifluorescence microscope (right panel). e) RIP using a rabbit polyclonal antibody targeting UPF1 was performed with HeLa cells expressing Globin PTC mRNA as well as Rex or Rev as indicated. Immunoprecipitated RNA (Globin PTC) were quantified by RTqPCR. For each condition, the relative enrichment of Globin PTC RNA associated to UPF1 compared to control conditions (pCMV) was displayed in the graph. f) Same as E with cells expressing globin WT mRNA. g) same as E with the quantification of endogenous mRNA gadd45a, smg5 and gapdh. h) Representative western blot controlling the RIP experiments: Rex and Rev proteins expression was monitored in the whole cell extract (INPUT) as well as UPF1 in immunoprecipitations.

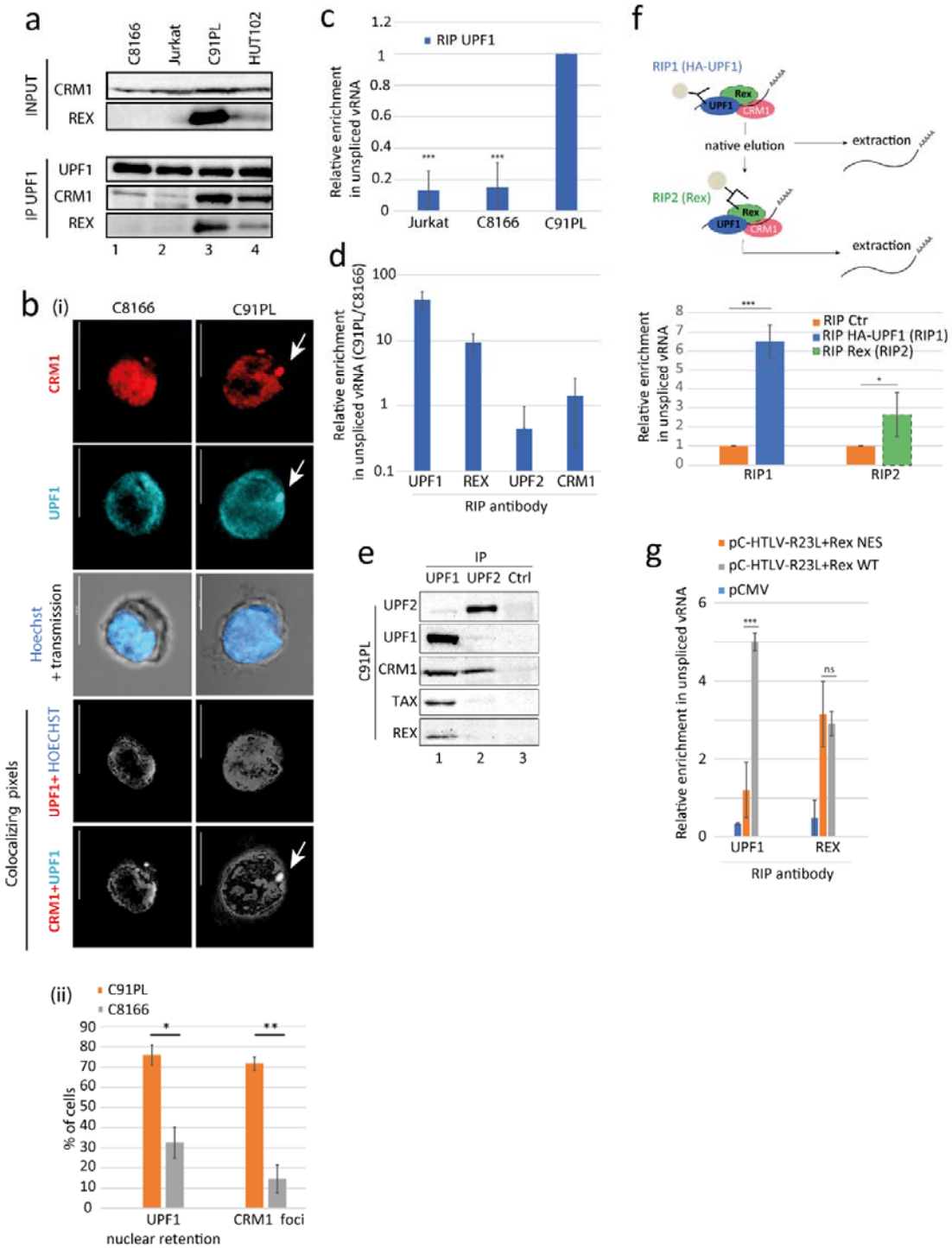

Figure 5: Rex/CRM1/UPF1 complex drives the loading of UPF1 on vRNA.

a) coIP experiments in the indicated lymphocytes cells extracts. IP were performed using rabbit polyclonal antibodies against UPF1. Proteins revealed by western blot are indicated on the side. b) (i) Confocal microscopy experiments were performed in C91PL and C8166 lymphocytes. CRM1 and UPF1 were revealed. The arrow shows a representative example of the CRM1 and UPF1 super foci (surface >= 1% total surface). Images were acquired with a

x63 objective. Scale bar: 10µm. (ii) Quantitative analysis of the relative number of cells with UPF1 nuclear retention (left) or with at least one CRM1 foci. c) RIP using a rabbit polyclonal antibody targeting UPF1 were performed with Jurkat, C8166 or C91PL lymphocytes. Immunoprecipitated unspliced viral RNA (vRNA) was quantified by RTqPCR. The relative enrichment of vRNA associated to UPF1 in Jurkat and C8166 compared to C91PL was displayed in the graph. The relative amount of vRNA in the total extract before RIP is indicated in Supplementary Fig 4D. d) RIP experiments were carried out with the immunoprecipitation of UPF1, Rex, UPF2 or CRM1 as indicated in C91PL and in C8166 cells. The relative enrichment in vRNA in C91PL compared to C8166 is represented for each immunoprecipitated protein. e) coIP experiments in the C91PL cells extracts. IP were performed from the same extract using UPF1, UPF2 or a control antibody (Ctr). Proteins revealed by western blot were indicated on the side. f) Schematic diagram of the double RIP experiment performed in 293T cells co-transfected with the HTLV-1 WT molecular clone and a HA-UPF1 coding plasmid (upper panel). Quantification of the relative enrichment in vRNA after HA RIP targeting UPF1 (RIP1) and Rex RIP (RIP2) (lower panel) compared to RIP Ctr. g) RIP targeting UPF1, Rex or using a control antibody (as indicated) were performed with 293T cells transfected with HTLV-1 R23L molecular clone complemented with either Rex NES or Rex WT (orange and grey bars respectively). As a negative control, cells were transfected with an empty vector (blue bars). Immunoprecipitated RNA (vRNA) was quantified by RTqPCR. The graph displays the relative enrichment of vRNA associated to UPF1 or Rex compared to control antibody.

Figure 6

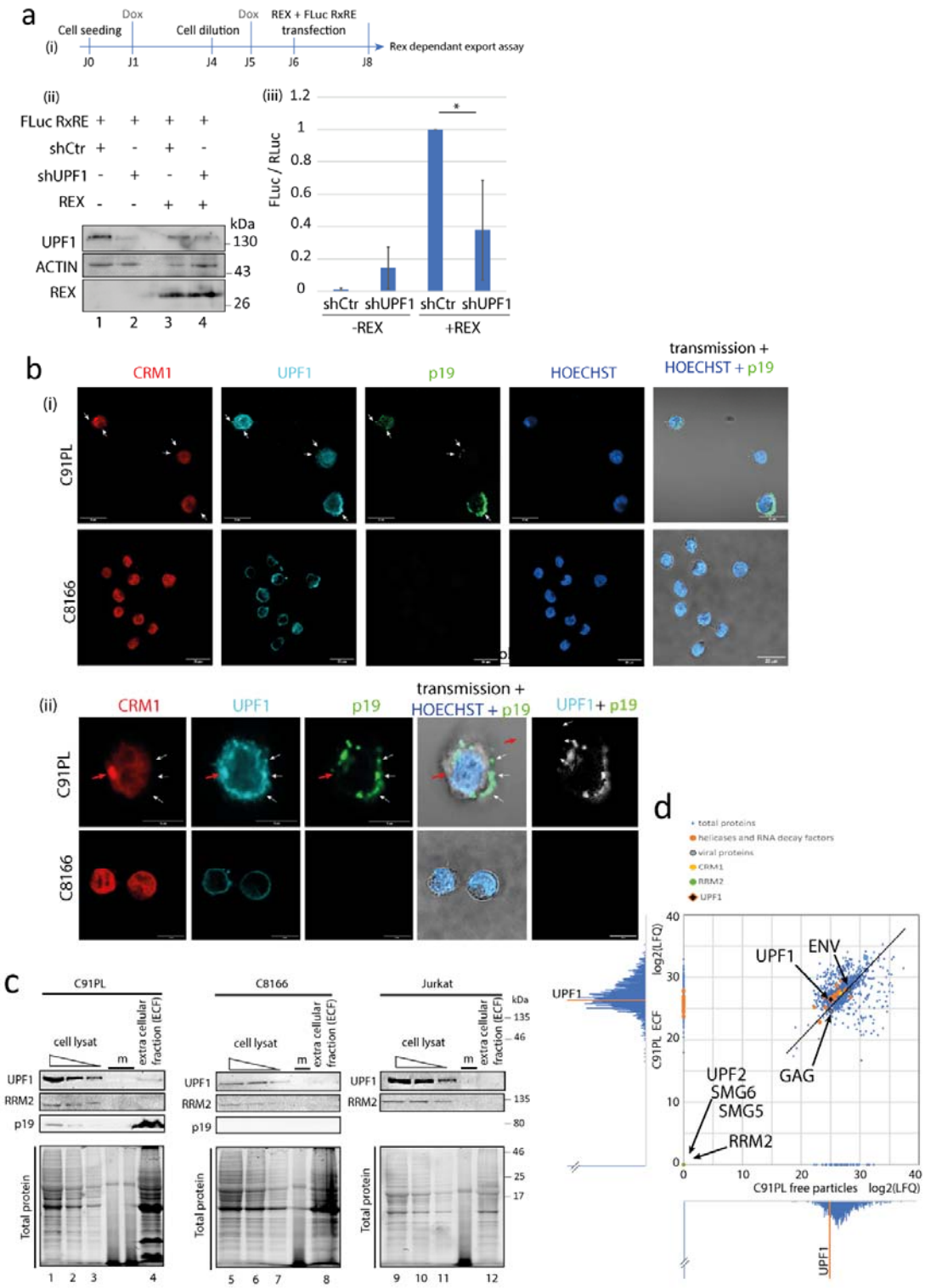

Figure 6: UPF1 is enriched in the extracellular particles produced by the virus.

a) (i) Schematic representation of the experiment. (ii) Protein expression in cell extracts used for dual luciferase assay was monitored by western blot. (iii) Dual luciferase assay was performed on shCtr or shUPF1 293T cells transfected with a Rex WT plasmid or an empty vector. Firefly luciferase as well as Renilla luciferase were quantified. Firefly (FLuc)/Renilla

(RLuc) ratio was plotted in a graph. b) Confocal microscopy experiments were performed in C91PL and C8166 lymphocytes. Panel (i): CRM1, UPF1 and p19 were revealed by IF. The arrow shows a representative example of p19 and UPF1 colocalization in C91PL. Images were acquired with a x20 objective. Scale bar: 50µm. Panel (ii): same as panel (i) with acquisitions with a-x63 objective (scale bar 10µm). White arrows show p19 foci. Red arrow shows the CRM1 superfoci. c) Extracellular fraction (ECF) containing the viral particles was collected from 15.10^6 of C91PL, C8166 and Jurkat cells and analysed (lanes 4, 8, 12). The presence of UPF1, RRM2 and p19 was evaluated by WB and total protein was monitored with stainless procedure (upper and lower panels respectively). Cells used to harvest the ECF were also lysed and monitored by WB after serial dilutions (equivalent to 4.10^6, 2.10^6 and 10^6 cells; lanes 1, 5, 9; 2, 6, 10; 3, 7, 11 respectively). d) Distribution of all the proteins quantified by mass spectrometry in the ECF (y axis) and in the “free particles” fraction (x axis) produced by C91PL cultures (in blue). Each coordinate corresponds to the mean of 3 independent experiments. On each axis, the density of proteins is represented. UPF1 position is indicated in orange on the density plots. Specific proteins (RNA decay factors partners involved in UPF1 dependant decay pathways, helicases, viral proteins, UPF1, RRM2, and CRM1) are indicated. Viral proteins GAG and ENV were found in both fractions, confirming the presence of viral particles.

Figure 7

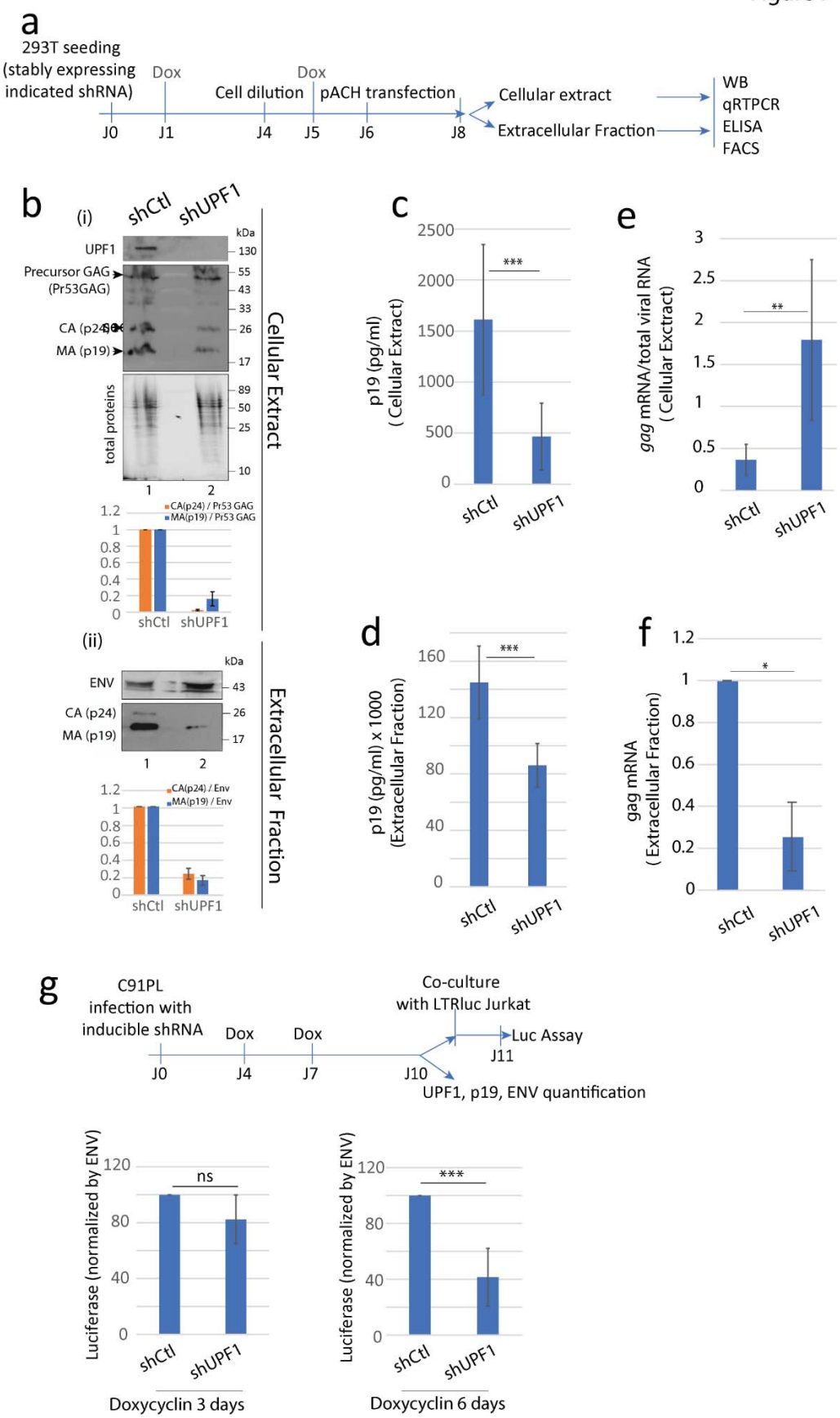
a
293T seeding
(stably expressing
indicated shRNA)
Dox
Dox
Cell dilution
pACH transfection
J0
J1
J4
J5
J6
J8
Cellular extract
Extracellular Fraction
WB
qRTPCR
ELISA
FACS
b
(i)
shCtl
shUPF1
kDa
UPF1
Precursor GAG
(Pr53GAG)
CA (p24)
MA (p19)
total proteins
130
55
43
33
26
17
89
50
25
10
1
2
CA(p24) / Pr53 GAG
MA(p19) / Pr53 GAG
shCtl
shUPF1
Cellular Extract
(ii)
ENV
CA (p24)
MA (p19)
43
26
17
CA(p24) / Env
MA(p19) / Env
Extracellular Fraction
c
p19 (pg/ml)
(Cellular Extract)
***
d
p19 (pg/ml) x 1000
(Extracellular Fraction)
***
e
gag mRNA/total viral RNA
(Cellular Exctract)
**
f
gag mRNA
(Extracellular Fraction)
*
g
C91PL
infection with
inducible shRNA
Dox
Dox
Co-culture
with LTRluc Jurkat
Luc Assay
J0
J4
J7
J10
J11
UPF1, p19, ENV quantification
Luciferase (normalized by ENV)
ns
***
Doxycyclin 3 days
Doxycyclin 6 days

Figure 7: UPF1 controls different steps of the viral replication cycle.

a) Schematic representation of the experiment. The same preparation of cell extracts and the corresponding extracellular fractions were used to perform western blot, qRTPCR and ELISA. FACS data are presented in Supplementary Fig5. b) Western blot was carried out on cellular extract (i) and on the corresponding extracellular fraction (ii). The recognized proteins were indicated on the left. The relative levels of the capsid (CA) and the matrix (MA) compared to the precursor GAG (i) or Env(ii) were evaluated after densitometry quantification using Imagelab software. c) ELISA spot assays (Zeptometrix) were performed with the cell extract of the indicated cells. MA(p19) quantification was plotted in bar plot. d) same as c with the extracellular fraction preparation. e) vRNA quantifications were performed by qRTPCR on cell extracts. Primers used were localized in the gag coding region. f) same as e) with the corresponding ECF preparation. g) upper panel: schematic representation of the viral transmission experiment. Lower panel: bar plot representing the luciferase levels expressed by $150x10^3$ infected Jurkat after 24h of co-culture with $50x10^3$ C91PL. C91PL were treated with doxycyclin for 3 days (1 treatment) or 6 days (2 treatments) in order to express the shRNA (control or against UPF1).

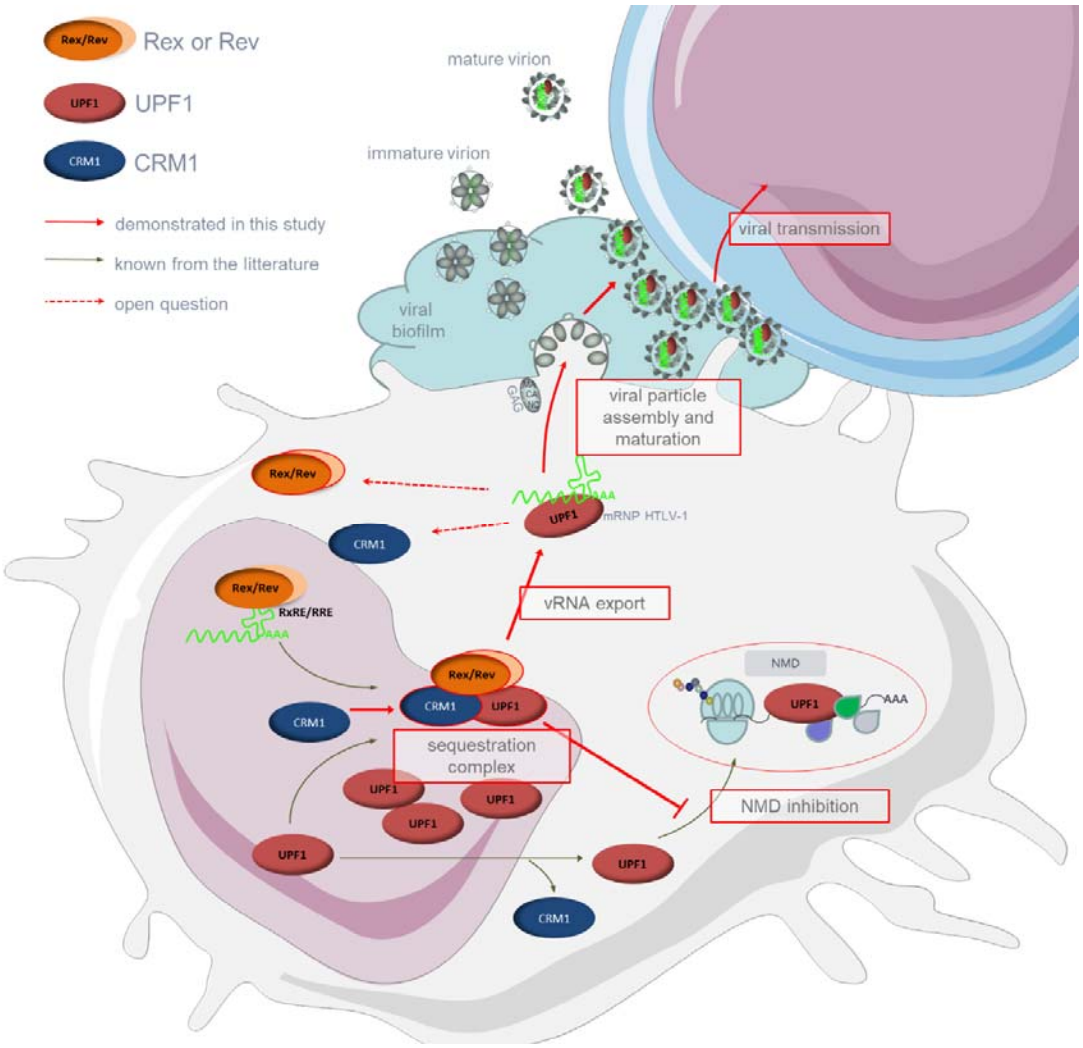

<u>Figure 8</u>: graphical abstract

During retroviral replication, the nuclear export unspliced vRNA is conducted via the hijacking of the exportin CRM1 by the viral protein Rex. in parallel, the RNA helicase UPF1 is naturally exported in a CRM1 dependent manner. In the cytoplasm it drives NMD, whose substrates include vRNA. Here we demonstrated that CRM1 hijacking by HTLV-1 Rex (and HIV Rev its functional homolog) provokes the formation of a tripartite complex Rex/CRM1/UPF1 associated with UPF1 nuclear redistribution. We correlated the formation of this sequestration complex with NMD inhibition. We also observed that UPF1 is part of the vRNA export complex leading to UPF1 loading onto vRNA (without NMD cofactors). In this context, UPF1 is driven in the viral particles where it plays critical role in virion assembly, maturation and ultimately viral infection. The red ovals in the mature virions represent UPF1. *Partly generated using Servier Medical Art, provided by Servier, licensed under a Creative Commons Attribution 3.0 unported license.*